JOURNAL OF PETROLOGY | VOLUME 49 | NUMBER 9 | PAGES 1619–1645 | 2008 | doi:10.1093/petrology/egn040

Processes and Sources during Late Variscan Dioritic–Tonalitic Magmatism: Insights from Plagioclase Chemistry (Gęsiniec Intrusion, NE Bohemian Massif, Poland)

A. PIETRANIK[1]* AND T. E. WAIGHT[2]

[1]INSTITUTE OF GEOLOGICAL SCIENCES, UNIVERSITY OF WROCŁAW, CYBULSKIEGO 30, 50-205 WROCŁAW, POLAND
[2]INSTITUTE FOR GEOGRAPHY AND GEOLOGY, GEOCENTER, UNIVERSITY OF COPENHAGEN, 1350 COPENHAGEN K, DENMARK

RECEIVED MAY 26, 2006; ACCEPTED AUGUST 14, 2008

The Gęsiniec Intrusion (Strzelin Massif, East Sudetes) (~307–290 Ma) is composed predominantly of dioritic to tonalitic rocks with $^{87}Sr/^{86}Sr$ ratios ranging from 0·7069 to 0·7080 and $\varepsilon_{Nd} = -3{\cdot}1$ to $-4{\cdot}2$, emplaced as post-collisional magmas following the Variscan orogeny. In situ *Sr isotope and trace element analyses of plagioclase were carried out on five diorite–tonalite samples with variable whole-rock $^{87}Sr/^{86}Sr$ compositions to constrain magma sources and elucidate magma chamber processes. Plagioclase is characterized by complex zoning patterns, such as patchy zoning, asymmetrical zoning and strong resorption between An-rich cores and more albitic rims. The range of Sr isotopic compositions recorded in plagioclase is 0·7069–0·7091, greater than that of the whole-rocks. No change in isotopic composition is observed across resorbed core–rim boundaries, as would be expected if the resorption was caused by magma mixing. Two samples are close to Sr isotopic equilibrium between plagioclase and the whole-rock. Three samples are isotopically heterogeneous and exhibit the largest variations in Sr isotope ratios within high-An plagioclase cores, associated with only slight resorption and almost no change in An content. Consequently, we interpret the core resorption to be due to decompression during emplacement of phenocryst-bearing magmas in the upper crust rather than to magma mixing, whereas we interpret the isotopic heterogeneity in the high-An plagioclase cores to be due to open-system processes in the lower crust. The trace element and Sr isotopic compositions of the high-An plagioclase cores provide an insight into the lower crustal processes that took place prior to decompression. We show that different diorite–tonalite types cannot be related to each other by assimilation–fractional crystallization processes and consequently they probably evolved as separate magma batches. Processes recorded in plagioclase core compositions include contamination by high $^{87}Sr/^{86}Sr$ crustal material and interaction with water-rich magma. The studied samples represent magmas that probably formed either by continuous differentiation and crustal contamination of originally more mafic magmas or by remelting of ~1·3–2·1 Ga basaltic materials in the lower crust. This study emphasizes the importance of integrating textural and in situ data to elucidate the processes that contribute to the formation of texturally and compositionally complex plagioclase crystals in plutonic rocks.*

KEY WORDS: *plagioclase chemistry; plagioclase zonation; diorite; tonalite; magma evolution; Variscan orogeny*

INTRODUCTION

Hornblende–biotite diorites and tonalites are widespread in orogenic areas worldwide, often occurring as dykes associated with more silicic plutons, or as enclaves within granitic batholiths (e.g. Blundy & Shimizu, 1991; Elburg, 1996; Cortesogno *et al.*, 1998; Altherr *et al.*, 1999; Bea *et al.*, 1999; Beddoe-Stephens, 1999; Roberts *et al.*, 2000; Pinarelli *et al.*, 2002; Castro *et al.*, 2003; Janoušek *et al.*, 2004). They are typically volumetrically minor and texturally variable, but are usually characterized by a similar mineral

*Corresponding author. E-mail: anna.pietranik@ing.uni.wroc.pl

assemblage (plagioclase, hornblende, biotite, quartz, rare pyroxene). They are characteristically emplaced at shallow crustal depths (7–15 km) as indicated by Al-in-hornblende barometery (e.g. Asrat *et al.*, 2004) or the presence of high-T mineral assemblages in the adjacent wall-rocks (e.g. Roberts *et al.*, 2000). However, they are thought to originate from magmas that differentiated at greater crustal depths and thus to represent an important 'window' into lower crustal magmatic processes (Roberts *et al.*, 2000).

Diorites and tonalites are often the least evolved rock types coexisting with larger granitic plutons and are, therefore, often interpreted as end-member magma compositions that interacted with the crust to produce a range of more felsic magmas. It is therefore important, before incorporating dioritic–tonalitic rocks into a general model of magma generation in orogenic areas, to understand their origins.

Initial Sr and Nd isotope compositions of dioritic–tonalitic rocks are often intermediate between those of the depleted mantle and the continental crust. Therefore, three potential magma sources have been proposed: enriched mantle (e.g. Altherr *et al.*, 1999; Janoušek *et al.*, 2000), more primitive mantle-derived magmas interacting with continental crust (e.g. Cortesogno *et al.*, 1998; Roberts *et al.*, 2000; Pinarelli *et al.*, 2002; Christofides *et al.*, 2007) and old, mafic lower crust (e.g. Jung *et al.*, 2002; Zhao *et al.*, 2007). A hybrid origin for dioritic–tonalitic rocks (via interactions between mantle- and crustal-derived materials) is supported by (1) a wide range of whole-rock Sr and Nd isotopic compositions within a single igneous complex that can be modeled by magma mixing or assimilation–fractional crystallization (AFC) processes (e.g. Oberc-Dziedzic *et al.*, 1996; Roberts *et al.*, 2000; Janoušek *et al.*, 2000; Pinarelli *et al.*, 2002) and (2) disequilibrium textures in minerals; for example, extensive resorption of An-rich plagioclase cores and subsequent crystallization of more albitic rims (e.g. Elburg, 1996; Janoušek *et al.*, 2004; Christofides *et al.*, 2007).

The variability of whole-rock Sr isotope compositions and presence of resorption textures in plagioclase from the dioritic–tonalitic rocks of the Gęsiniec Intrusion (Oberc-Dziedzic *et al.*, 1996) suggest that study of these rocks may potentially provide important petrogenetic information applicable to other dioritic–tonalitic intrusions. This study provides a detailed description of the textural, geochemical and Sr isotope variations within plagioclase, coupled with detailed field relations, petrography and whole-rock data. We use *in situ* isotope, major and trace element analyses of plagioclase, with a focus on the plagioclase composition before and after resorption, to reconstruct the crystallization history and identify the source materials that may have contributed to the dioritic–tonalitic magmas. We demonstrate that such a detailed approach is critical for the interpretation of isotopic and geochemical variations within the Gęsiniec Intrusion and, by extension, other intrusions of complex, hybrid origin.

REGIONAL GEOLOGY

The Strzelin Massif, in the eastern part of the Sudetes–Central European Varisicides, represents part of the Variscan orogen of Europe (Fig. 1). The Variscan orogeny resulted from the collision of Gondwana and Laurasia at *c.* 380–280 Ma. The Sudetes are interpreted to have formed by accretion of five major terranes, derived from the Gondwana supercontinent (Aleksandrowski & Mazur, 2002). The Strzelin Massif is located at the contact between the Brunovistulian and Moldanubian terranes (Oberc-Dziedzic *et al.*, 2003), and crops out as a north–south-elongated block 35 km south of Wrocław between 50°38' and 50°46'N, and 17°00' and 17°10'E. The pre-Variscan basement of the Strzelin Massif includes gneisses and amphibolites [the magmatic protolith of the Strzelin gneiss has been dated to 600–568 Ma by sensitive high-resolution ion microprobe (SHRIMP) U–Pb zircon dating (Oberc-Dziedzic *et al.*, 2003)], Lower Paleozoic schists and Devonian quartzites (Fig. 1b; Oberc-Dziedzic, 1999*a*). This basement was metamorphosed to amphibolite facies during the Variscan orogeny and subsequently intruded by late- to post-collisional granitoids. All the granitoids occur as small, isolated bodies, mostly stocks up to 1 km in diameter and dykes up to 200 m thick (Fig. 1c). They include biotite granites, granodiorites, tonalites, quartz diorites, diorites and two-mica granites; rare gabbros are also observed in bore-hole material (Oberc-Dziedzic, 1999*b*, 2002). The largest granitic body is the Strzelin Intrusion (Oberc-Dziedzic, 1999*a*). The Gęsiniec Intrusion, the subject of this study, is the largest (>200 m thick) diorite–tonalite dyke in the area, and cuts Pre-Variscan basement (Fig. 1c).

A Rb/Sr whole-rock isochron for biotite granite from the Strzelin Intrusion yielded an age of 347 Ma with an initial $^{87}Sr/^{86}Sr$ ratio of $0{\cdot}7053 \pm 2$ (Oberc-Dziedzic *et al.*, 1996). This granite contains enclaves of dioritic and tonalitic rocks, suggesting that the diorites and tonalites are therefore older than 347 Ma (Oberc-Dziedzic *et al.*, 1996). However, recent U–Pb zircon evaporation data have yielded ages of 291 Ma for both the biotite granite from the Strzelin Intrusion and the tonalite from the Gęsiniec Intrusion (Turniak *et al.*, 2006).

ANALYTICAL METHODS

Whole-rock geochemistry

Major and trace element whole-rock geochemistry was determined by X-ray fluorescence (XRF) at the Geocenter, Copenhagen using standard methods described by Kystol & Larsen (1999). The accuracy of analyses was checked on five international reference materials measured

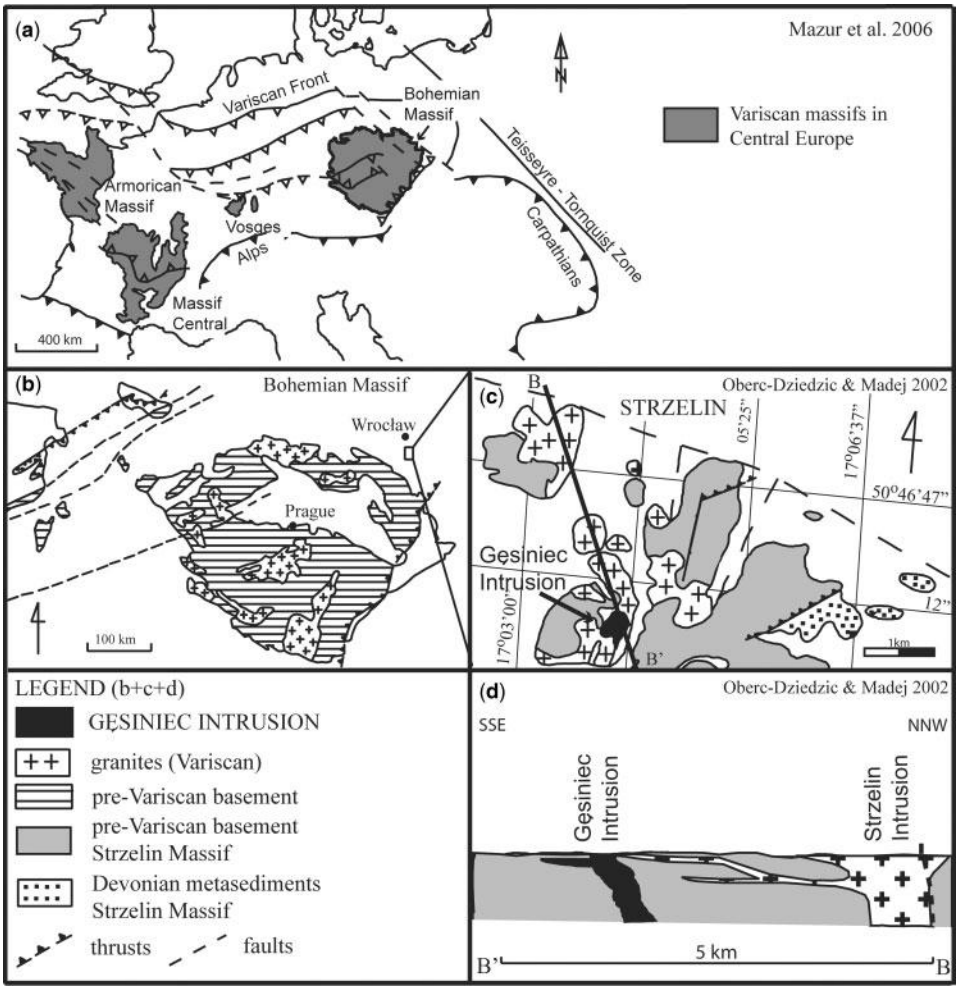

Fig. 1. Geological setting of the Bohemian Massif, the Strzelin Massif and the Gęsiniec Intrusion. (a) Location of the Bohemian Massif in Central Europe (modified after Mazur *et al.*, 2006); (b) location of the Strzelin Massif relative to the Bohemian Massif (modified after Mazur *et al.*, 2006); (c) simplified geological map of the northern part of the Strzelin Massif (modified after Oberc-Dziedzic & Madej, 2002); (d) simplified cross-section as indicated in (c) (modified after Oberc-Dziedzic & Madej, 2002).

at the same time as the samples (BHVO-1, BHVO-2, DISCO1, GH, AGV2) and was usually within 5% SE for trace elements and 0·5% SE for major elements.

Mineral chemistry

Two electron microprobes were used in this study: a JEOL JXA8200 Superprobe at the Geocenter Copenhagen and a CAMECA SX100 at the Institute of Mineralogy, University of Hannover. Analytical conditions for both instruments were 15 kV acceleration voltage, 10 nA sample current, focused beam, and 10 s counting time for peak and background. Duplicate analyses of plagioclase from the same rock type at the two laboratories gave identical results.

Laser ablation-inductively coupled plasma mass spectrometry (ICPMS)

Laser ablation ICPMS was used to determine the trace element contents of representative plagioclase crystals from each sample. Analyses were carried out using a 266 nm Nd–YAG CETAC laser coupled to a Perkin Elmer Quadropole ICPMS system housed at GEUS, Copenhagen. Operating conditions were pulse repetition rate 20 Hz and spot size 50 μm. Most data were collected as 60s line scans parallel to homogeneous zones identified using back-scattered electron images. Backgrounds were measured as gas blanks for 20 s prior to ablation. Glass NIST SRM 610 (Pearce *et al.*, 1997) was used as an external standard to correct for laser-induced elemental fractionation and was measured at the beginning of data acquisition and between each group of 10 line scans. To eliminate the effects of drift in the instrument response and to correct for different volumes of material ablated from standard and sample, measurements of both the standard and the sample were normalized to calcium contents in plagioclase, obtained from electron microprobe measurements, using the methods described by Košler (2001).

To check on the precision and accuracy of measurements the NIST SRM 612 glass was analysed as an unknown (see Appendix, Table A1). Most of the elements analyzed were reproduced to within ±8–20% of the recommended element concentrations (2 SE).

Isotope techniques

All sample processing and measurements of isotopic compositions were carried out in the laboratories of the Geocenter, Copenhagen.

Whole-rock and biotite separates

Whole-rock powders (*c.* 100 mg) and biotite mineral separates (*c.* 20–50 mg) were dissolved in Teflon beakers in high-pressure bombs at 200°C for several days in a progression of HF, HCl and HNO_3. After dissolution samples were checked to ensure complete dissolution and then quantitatively split into isotope composition (IC) and isotope dilution (ID) aliquots; mixed $^{84}Sr/^{87}Rb$ and $^{150}Nd/^{149}Sm$ spikes were added to the latter.

Rb, Sr and the rare earth elements (REE) were separated using HCl and conventional cation exchange columns (AG50-X8 resin). Rb and Sr were further purified using Sr-spec resin.

Microdrill samples

Plagioclase samples were collected using methods similar to those of Waight *et al.* (2000). Plagioclase was sampled using a manual drill (diameter 500–800 μm); the depth of drilling could not be strictly controlled and varied from *c.* 100 to ~500 μm. It was not possible to determine sample weights precisely because of static problems, but they ranged from *c.* 0·5 to 1·5 mg. Samples were dissolved in HF, HCl and HNO_3 on a hot plate and spiked with a diluted $^{84}Sr/^{87}Rb$ spike. The use of a mixed spike ensures that Rb–Sr ratios can be determined independently of sample weight. Samples were processed first through Sr-spec resin (to purify Sr) and the waste was processed through a miniaturized version of the whole-rock chemistry to purify Rb. Sr blanks were below 500 pg and, assuming a blank composition of 0·72, result in blank corrections smaller than the analytical uncertainty.

Analytical techniques

Sr samples were loaded on Ta filaments with a TaF activator and analyzed by thermal ionization mass spectrometry in multi-dynamic mode on a VG54 system. Rb samples were taken up in 0·2M HCl, doped with Zr and analyzed on an Axiom MC-ICPMS system using techniques described by Waight *et al.* (2002). Nd was run on a bulk REE solution on an Axiom MC-ICPMS system using methods similar to those described by Luais *et al.* (1997).

Replicate measurements of SRM987 over the period of this study gave $^{87}Sr/^{86}Sr = 0{\cdot}71023 \pm 3$ (2σ, $n = 11$), natural Rb doped with Zr gave $^{85}Rb/^{87}Rb = 0{\cdot}3856 \pm 6$ (2σ, $n = 17$). Reproducibilities (2SD) for the initial $^{87}Sr/^{86}Sr$ and ε_{Nd} for the whole-rock and microdrill samples are taken to be 0·01% and ±0·3 ε units, respectively.

THE GĘSINIEC INTRUSION: FIELD RELATIONSHIPS AND PETROGRAPHY

The rocks of the Gęsiniec Intrusion are well exposed in an active quarry and are typical of diorite–tonalite rocks elsewhere in the Strzelin Massif (Oberc-Dziedzic, 2002). The Gęsiniec Intrusion is a compositionally zoned, sheet-like, intrusive body (*c.* 0·2–0·4 km in diameter) composed mainly of quartz diorite, diorite, tonalite (Fig. 2) and subordinate granodiorite crosscut by a number of two-mica granite dykes (10 cm–20 m thick). Some of the diorites show evidence of mingling with a granodioritic magma; this has resulted in the formation of biotite tonalites enriched in K-feldspar (Fig. 2). The mingling indicates interaction between partially to nearly crystallized magmas, probably at the depth of final emplacement (Pietranik & Koepke, in preparation). Because our aim was to constrain the evolution of the dioritic–tonalitic magmas before their final emplacement, all samples affected by magma mingling were excluded from this study. After microscopic examination of *c.* 50 samples, 15 samples of not-mingled diorites, quartz diorites and tonalites were chosen for further study. The samples were subdivided in six types, each including a spectrum of rocks from diorite to tonalite but termed quartz diorite for simplicity: (1) fine-grained quartz diorite (FGD); (2) leucocratic poikilitic quartz diorite (LPD); (3) melanocratic quartz diorite (MD); (4) leucocratic medium-grained quartz diorite (LMGD); (5) leucocratic coarse-grained quartz diorite (LCGD); (6) melanocratic coarse-grained quartz diorite xenoliths (MCGD-x). Generally, those rocks that classify modally as diorites to tonalites are classified as monzodiorites and quartz monzodiorites on the basis of their whole-rock geochemistry (Fig. 2).

Field relationships and the petrographic characteristics of each subtype are summarized in Table 1 and Fig. 3. The pressure of crystallization calculated using the Al-in-hornblende barometer (Anderson & Smith, 1995) for hornblende rims varies from 1·8 to 3 kbar (see the Supplementary Data, which are available for downloading at http://www.petrology.oxfordjournals.org).

WHOLE-ROCK AND Sr–Nd ISOTOPE GEOCHEMISTRY

Seven representative whole-rock samples were analyzed for their trace element and five for their Sr–Nd isotope

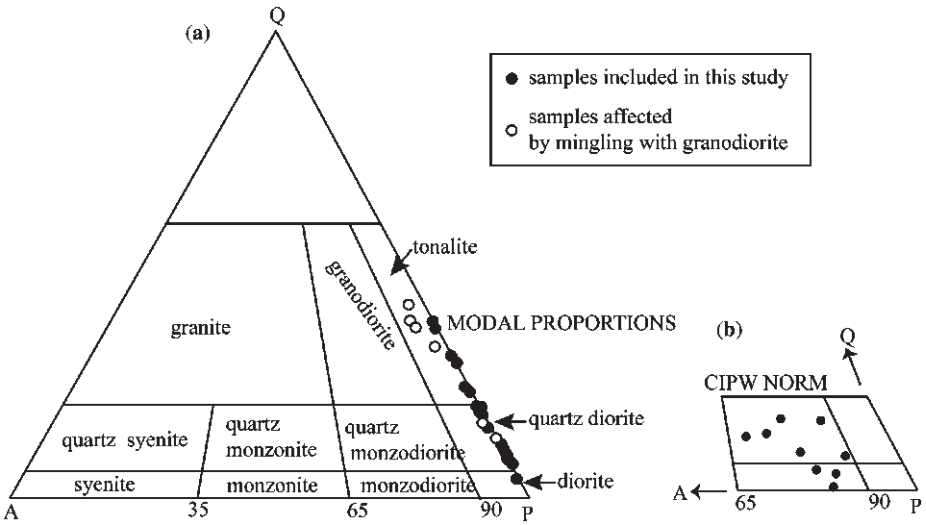

Fig. 2. Classification of rocks from the Gęsiniec Intrusion in the QAP diagram: (a) the simplified QAP ternary shows the modal composition; (b) the inset on the right-hand side illustrates the CIPW normative composition.

composition. The whole-rock chemistry of the xenolith samples (MCGD-x) was not determined because of the small sample size.

Major and trace elements

Major and trace element compositions of the quartz diorites are presented in Table 2. They exhibit a range of silica (52–57 wt %) and MgO (3–8 wt %) contents. Primitive mantle-normalized multi-element diagrams for the different types are characterized by broadly similar trends of enriched incompatible elements and negative Sr and Ti anomalies (Fig. 4a). All rock types are characterized by the absence of significant fractionation of the light REE (LREE) and large ion lithophile elements (LILE) from high field strength elements (HFSE) (e.g. Nb/Ce_{CN} varies from 0·7 to 1·7, Table 2). The REE patterns are characterized by strong LREE enrichment and negative Eu anomalies (Fig. 4b). Two broad geochemical groups occur, distinguished by relatively high or low concentrations of P_2O_5, Ba, REE and Y. The high-P_2O_5 group is also characterized by relatively high TiO_2, Nb and Ta. Single rock types vary also in their K, Mg, Ca, Cr, Ni, Rb and Sr contents.

The quartz diorite samples do not display clear linear trends on Harker diagrams or trace element vs trace element plots. However, when samples with high Mg, Cr, Ni contents are excluded as probable cumulates, approximately linear trends ($R^2 \sim 0{\cdot}5$) are evident for the remaining samples. For example, SiO_2 correlates negatively with Al_2O_3, FeO, CaO, MgO, Sr and Eu, whereas MgO correlates positively with CaO, Sr and negatively with Nb and Ta (Fig. 5). No correlation is observed between differentiation indexes such as SiO_2 or MgO and many incompatible elements such as P_2O_5, TiO_2, K_2O, REE, Y, Rb and Ba. However, P_2O_5 correlates positively with many of them [K_2O, TiO_2, Nb, Ta, middle REE (MREE), Y, Rb; R^2 varying from 0·5 to 0·8; Fig. 5].

Rb–Sr isochrons

To calculate the initial Sr and Nd isotope compositions of whole-rocks (WR) and plagioclase, isochrons based on mineral (biotite plus drilled plagioclase) and whole-rock data were constructed for samples of quartz diorite using the Isoplot/Ex program version 3.07 (Ludwig, 2004). The resulting isochron and errorchrons yield ages ranging from ~281 ± 26 Ma to 307·0 ± 4·8 Ma (Table 3). All calculated ages are significantly younger than the previous estimate of 347 Ma (Oberc-Dziedzic *et al.*, 1996) but are in broad agreement with zircon U–Pb evaporation ages of 291 Ma (Turniak *et al.*, 2006). Recalculation of the Sr isotopic data in this study to 347 Ma, 307 Ma or 291 Ma results in little change in the initial $^{87}Sr/^{86}Sr$ in plagioclase because of its low Rb/Sr. The effect for whole-rocks is much larger and results in much larger contrasts between Sr isotopic compositions for whole-rocks and plagioclase feldspars at 347 Ma than at 291–307 Ma. Consequently, all isotope data in this study, including the previously published data of Oberc-Dziedzic *et al.* (1996), have been age corrected to 295 Ma, the isochron age of the LMGD sample (Table 3).

Initial isotope compositions

Initial isotope compositions for whole-rock samples vary from $\varepsilon_{Nd} = -4{\cdot}22$ to $-2{\cdot}91$ and from $^{87}Sr/^{86}Sr_{295} = 0{\cdot}70691$ to 0·70805 (Fig. 6, Table 4). The quartz diorite sample with high Cr and Ni contents (MD, Table 4) has an intermediate $^{87}Sr/^{86}Sr_{295}$ of 0·70739 and low ε_{Nd} of −3·61. The quartz diorite sample with relatively unradiogenic Sr and the

Table 1: Petrographic characteristics and mineral compositions of the six diorite–tonalite types defined in this study

Rock type	Occurrence	Characteristic texture	Rock-forming minerals	Accessory minerals	Secondary minerals
Fine-grained quartz diorite (FGD)	outer parts of the intrusion	equigranular to porphiritic, fine grained	plagioclase (45–50%), biotite (20–25%), amphibole (ferropargasite, pargasite, ferro-tschermakite, hornblende, Al_{TOT}=1·4–2·0) (10–15%), quartz (20–25%)	acicular apatite, ilmenite, zircon	very rare chloritized amphibole and biotite
Leucocratic poikilitic quartz diorite (LPD)	dominant type, in contact with fine-grained diorite and quartz diorite	biotite poikilocrysts (up to 8 mm) enclosing plagioclase and apatite, contains scarce aggregates of euhedral coarse-grained amphibole (pargasite) grains enclosing acicular apatite	plagioclase (45–50%), biotite (20–25%), amphibole (ferropargasite, pargasite, ferro-tschermakite, hornblende, Al_{TOT}=1·6–2·1) (10–15%), quartz (15–25%)	acicular apatite, euhedral titanite, ilmenite, zircon	rare chloritized amphibole and biotite, rare sericitized plagioclase
Melanocratic quartz diorite (MD)	dykes up to several meters thick within LPD	medium-grained domains dominated by mafic minerals (~60%) and scarce fine-grained domains dominated by plagioclase (~90%), occurrence of resorbed biotite in amphibole and late biotite crystallized after plagioclase and amphibole	amphibole (Mg-hornblende, cummingtonite, actinolite, Al_{TOT}=0·6–1·6) (30–40%), plagioclase (15–20%), biotite (30%), quartz (15–20%)	coarse-grained apatite, ilmenite, zircon, monazite, FeS	interstitial carbonates, NOT actinolite rims on amphibole rare sericitization of plagioclase, biotite chloritized
Leucocratic medium-grained quartz diorite (LMGD)	dominates the inner part of the Gęsiniec Intrusion	equigranular; medium-grained, amphibole contains small plagioclase grains	plagioclase (45–50%), amphibole (Mg-hornblende, Al_{TOT} =0·9–1·8) (25–35%), biotite (13–20%), quartz (15–18%)	coarse-grained apatite, titanite, ilmenite, zircon	rare chloritized amphibole and biotite, rare sericitized plagioclase
Leucocratic coarse-grained quartz diorite (LCGD)	blocks (up to 1 m) with diffuse boundaries within LPD	clots of mafic minerals, fine-grained interiors of amphibole composed of biotite, actinolite and chlorite	plagioclase (45–55%), amphibole (tschermakite, Mg-hornblende, actinolite, Al_{TOT}=0·6–2·1) (10–20%), biotite (10–15%), quartz (15–30%)	coarse-grained ilmenite, apatite, titanite, zircon, anhedral allanite	chlorite and actinolite only in fine-grained interiors of amphibole crystals
Melanocratic coarse-grained quartz diorite xenolith (MCGD-x)	occur only as small, enclave- like bodies (up to 10 cm in size) within LMGD, their grain size is coarser than that of the host	equigranular; coarse-grained, very rich in accessory minerals, mainly titanite	Plagioclase (30–40%), amphibole (Mg- hornblende, actinolite, Al_{TOT}=0·6–1·9) (30–40%) biotite (25–35%), quartz (10–15%)	titanite surrounding ilmenite, apatite, zircon, allanite	actinolite rims on amphibole, very rare chloritized biotite and very rare sericitized plagioclase

Modes are given in parenthesis in 'Rock-forming minerals' columns. Nomenclature of amphiboles after Leake *et al.* (1997). The numbers in parenthesis after amphibole classification correspond to total Al recalculated on the basis of 15 cations (minus Ca, Na, K) per formula unit.

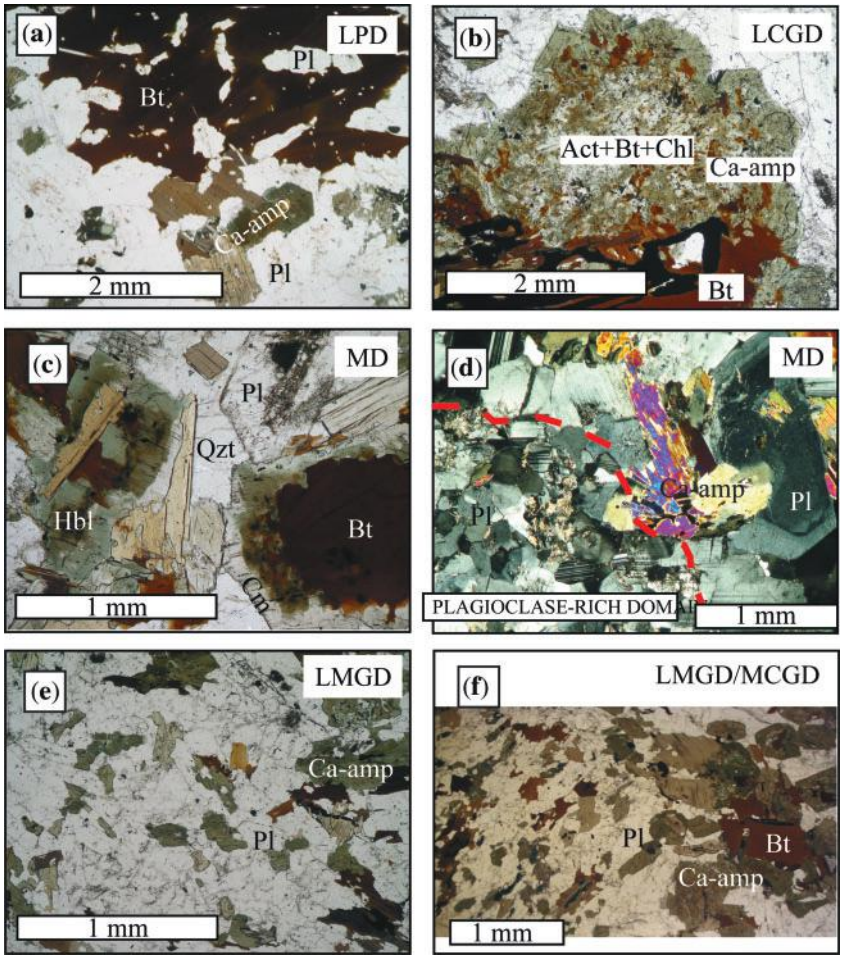

Fig. 3. (a) LPD, leucocratic poikilitic quartz diorite: microscope view of biotite phenocryst and smaller amphibole (plane-polarized light; PPL); (b) LCGD, leucocratic coarse-grained quartz diorite: microscope view of the altered interior of an amphibole grain with a thin unaltered rim (PPL); (c) MD, melanocratic quartz diorite: microscope view of resorbed biotite grains in the interiors of amphibole grains (PPL); (d) MD, melanocratic quartz diorite: contact of fine-grained plagioclase-rich domain and medium-grained tonalite, microscope (cross-polarized light); (e) LMGD, leucocratic medium-grained quartz diorite: microscope view of typical hornblende crystals containing small plagioclase grains (PPL); (f) MCGD-x, melanocratic coarse-grained quartz diorite xenolith in LMGD, microfiche (PPL).

most radiogenic Nd (LPD) has a similar SiO_2 and MgO content to the quartz diorite sample with the most radiogenic Sr and the least radiogenic Nd (LCGD, Fig. 6).

The range of Sr isotope compositions observed in this study is similar to those presented by Oberc-Dziedzic *et al.* (1996; Fig. 6). Only the least radiogenic samples were not encountered in our study, possibly because they were already quarried out or because of inter-instrumental bias.

PLAGIOCLASE: MORPHOLOGY AND AN CONTENT

In situ analyses of plagioclase were conducted for five quartz diorite types to cover the observed range of WR Sr and Nd isotope ratios. Numerous plagioclase grains were characterized from each of the quartz diorite samples on the basis of optical microscope investigations, BSE imaging and An contents (Table 5).

Zonation styles and anorthite content

The zonation patterns within plagioclase crystals are variable and complex and include: (1) resorbed An-rich cores surrounded by more albitic rims, sometimes with asymmetric zonation from rim to rim (Fig. 7a); (2) patchy zoned interiors (Fig. 7b); (3) albite-rich interiors, partly surrounded by a zone richer in An (Fig. 7c); (4) rounded, An-rich cores surrounded by plagioclase with a similar An content (Fig. 7d). However, we consider that most of this apparent complexity [types (1)–(3)] is due to late resorption leading to the formation of strongly embayed plagioclase interiors as schematically illustrated in Fig. 7. Resorption appears to vary in intensity, and

Table 2: Whole-rock major and trace element data

	FGD1	FGD2	LPD	MD2	MD1	LMGD2	LMGD1	LCGD
wt %								
SiO_2	51·42	57·86	55·57	56·19	55·04	57·15	53·97	56·55
TiO_2	1·85	1·33	1·61	1·16	1·5	2·41	1·19	2·21
Al_2O_3	17·41	16·47	16·90	13·37	12·53	16·72	16·83	15·99
Fe_2O_3	10·35	7·72	9·02	9·68	10·83	7·33	7·96	8·63
MnO	0·17	0·13	0·14	0·18	0·2	0·13	0·14	0·18
MgO	4·05	3·41	3·08	7·62	8·37	3·24	4·8	3·00
CaO	7·76	6·12	6·37	5·13	4·85	6·73	8·14	5·84
Na_2O	3·53	2·90	3·33	2·13	1·73	3·33	3·01	2·86
K_2O	1·90	1·92	2·34	2·37	2·59	1·49	1·24	2·37
P_2O_5	0·86	0·31	0·73	0·4	0·45	0·47	0·45	0·88
LOI	0·57	0·88	0·86	1·02	0·81	0·72	2	0·85
Total	99·88	99·29	99·95	99·25	98·90	99·70	99·73	99·35
ppm								
Sc	20·5	15·4	16·2	19·6	21·4	15·7	21	17·1
V	164·8	122·9	133·9	138·8	151·2	185·5	153	173·6
Cr	23·3	60·6	8·5	424·2	475·6	19·7	90	2·5
Co	40·8	42·9	61·1	55·4	67·0	48·2	24·8	52·9
Ni	25·9	35·4	16·1	126·2	139·4	25·4	19·8	14·5
Cu	34·0	20·9	36·2	61·0	80·4	33·6	59	32·4
Rb	66·1	94·6	93·2	81·1	96·7	51·2	54·6	109·7
Sr	368·3	80·3	346·6	231·8	211·7	334·5	374·7	305·9
Y	49·4	342·6	47·5	32·2	32·3	22·3	30	42·7
Zr	—	—	—	—	—	—	202·3	—
Nb	40·8	35·3	40·6	23·5	30·0	36·8	25·3	48·3
Cs	0·8	1·8	1·5	3·0	10·1	1·6	4·3	3·0
Ba	586·6	635·5	663·8	446·0	463·7	413·2	322·2	629·9
La	51·1	55·1	44·8	42·5	41·9	24·3	39·9	49·1
Ce	118·5	112·7	101·5	83·0	83·7	51·8	91·1	104·3
Pr	16·0	13·7	13·5	10·4	10·2	7·0	11·6	13·3
Nd	61·0	49·1	51·1	37·7	37·6	26·9	43·6	49·1
Sm	11·8	9·3	10·0	7·3	7·3	5·3	7·3	9·6
Eu	2·6	2·1	2·1	1·4	1·4	1·3	1·8	1·8
Gd	11·1	8·8	9·4	6·9	6·9	5·0	6·7	9·2
Tb	1·6	1·2	1·4	1·0	1·0	0·7	1	1·3
Dy	8·7	6·8	7·8	5·5	5·5	3·9	5·3	7·3
Ho	1·7	1·3	1·5	1·1	1·1	0·8	1	1·4
Er	4·5	3·4	4·2	3·0	2·9	2·0	2·9	3·7
Tm	0·6	0·5	0·6	0·4	0·4	0·3	0·4	0·5
Yb	3·8	3·2	3·6	2·7	2·5	1·8	2·6	3·2
Lu	0·6	0·5	0·5	0·4	0·4	0·3	0·4	0·5
Ta	2·0	2·2	2·4	1·3	1·6	3·0	1·6	3·3
Pb	6·8	5·8	6·6	5·5	4·4	8·0	1·5	5·5
Th	1·3	7·1	7·0	7·9	7·7	3·0	7·1	6·4
U	0·9	3·3	1·2	1·2	1·0	2·0	2·3	18·1

(continued)

Table 2: Continued

	FGD1	FGD2	LPD	MD2	MD1	LMGD2	LMGD1	LCGD
La/Yb_{CN}	9·33	12·1	8·57	10·9	11·42	9·45	10·69	10·52
Nb/Ce_{CN}	0·84	0·76	0·98	0·69	0·88	1·74	0·68	1·14
Eu/Eu^{*}_{CN}	0·68	0·70	0·66	0·61	0·6	0·79	0·8	0·57

'-', element not analyzed. LOI, loss on ignition. LREE enrichment, Nb/Ce ratios and Eu anomaly ($Eu/\sqrt{Sm \times Gd}$) normalized to chondrite (normalizing values from Anders & Grevesse, 1989).

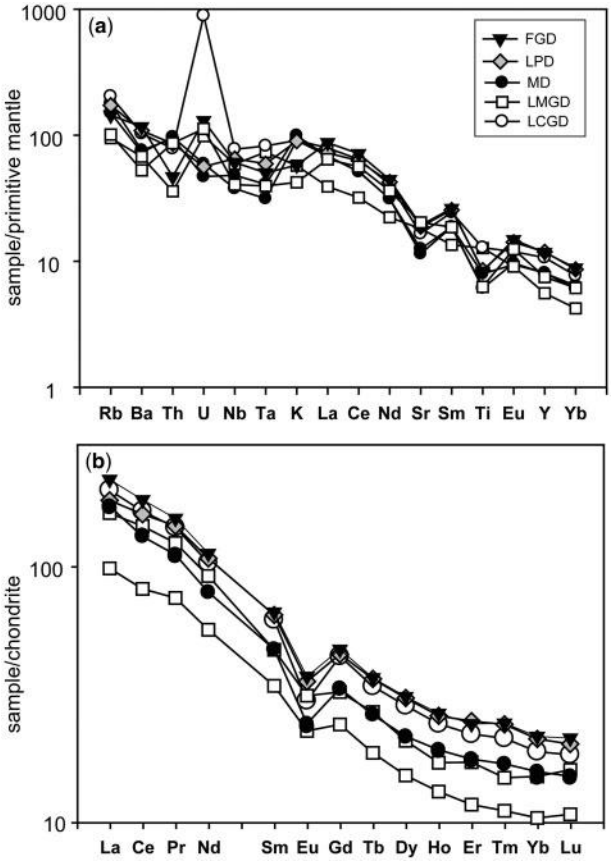

Fig. 4. (a) Primitive mantle normalized (normalizing values from Sun & McDonough, 1989) incompatible trace element diagram for quartz diorites; (b) chondrite-normalized REE patterns (normalizing values from Anders & Grevesse, 1989).

is most extreme when previously crystallized plagioclase zones have been completely removed (Fig. 7c) or are preserved only as isolated patches (Fig. 7b). Resorption is often focused along the axis of plagioclase grains, resulting in their division into two separate crystals with asymmetrical zonation (Fig. 7a; one half of a divided crystal). Taking the effects of the resorption into account, the plagioclase zonation patterns are simple and well correlated, and thus potentially provide important records of magma chamber processes. Based on these textural observations, plagioclase crystals can be divided into two or three texturally and compositionally distinct parts, each separated by a resorption event: cores (Zone A), mantles (Zone B) and rims (Zone C, Fig. 7, Table 5). The major element compositions of each zone are given in the Supplementary Data.

Zone A. This is found in only two quartz diorite types (MD and LCGD, Table 5); its outer boundary is always rounded by resorption. Zone A has a relatively constant composition ($An_{59–66}$); however, a sharp increase to $An_{67–72}$ is observed across the resorbed boundary (Fig. 7a and d, Table 5).

Zone B. This occurs in all except the smallest plagioclase grains (<500 μm) in all lithologies, either surrounding Zone A or forming the innermost core of the crystal when Zone A is absent (Fig. 7). It is normally zoned from $An_{54–72}$ to *c*. $An_{26–43}$. Plagioclase from MCGD-x exhibits lower An concentrations in Zone B compared with all other quartz diorites.

Zone C. The Zone B–Zone C boundary is characterized by extensive resorption and a slight increase in An content to An_{47}. The resorption event predominantly affects the inner parts of the crystals (Zones A and B), whereas most of the original euhedral form of the outer Zone B–Zone C boundary is preserved (Fig. 7) and associated with an increase in An content of ~5%. Zone C ($An_{20–47}$) forms rims on all plagioclase grains and fills the embayments, representing new growth of plagioclase following resorption. The range of An content of plagioclase in the embayments is $An_{20–47}$, whereas it is $An_{30–43}$ in the rims. The embayments are also often filled with rounded, irregular inclusions of other minerals surrounded by plagioclase of Zone C composition (e.g. Fig. 7d), representing recrystallized melt inclusions. Zone C is typically normally zoned but thicker zones may exhibit complex oscillatory zoning with wavy boundaries between zones or constant An contents (~An_{45}).

Despite the random plagioclase profiles represented in thin section, correlation of zones between different plagioclase grains within each type is excellent; for example, Zone A occurs in all larger grains in LCGD and MD,

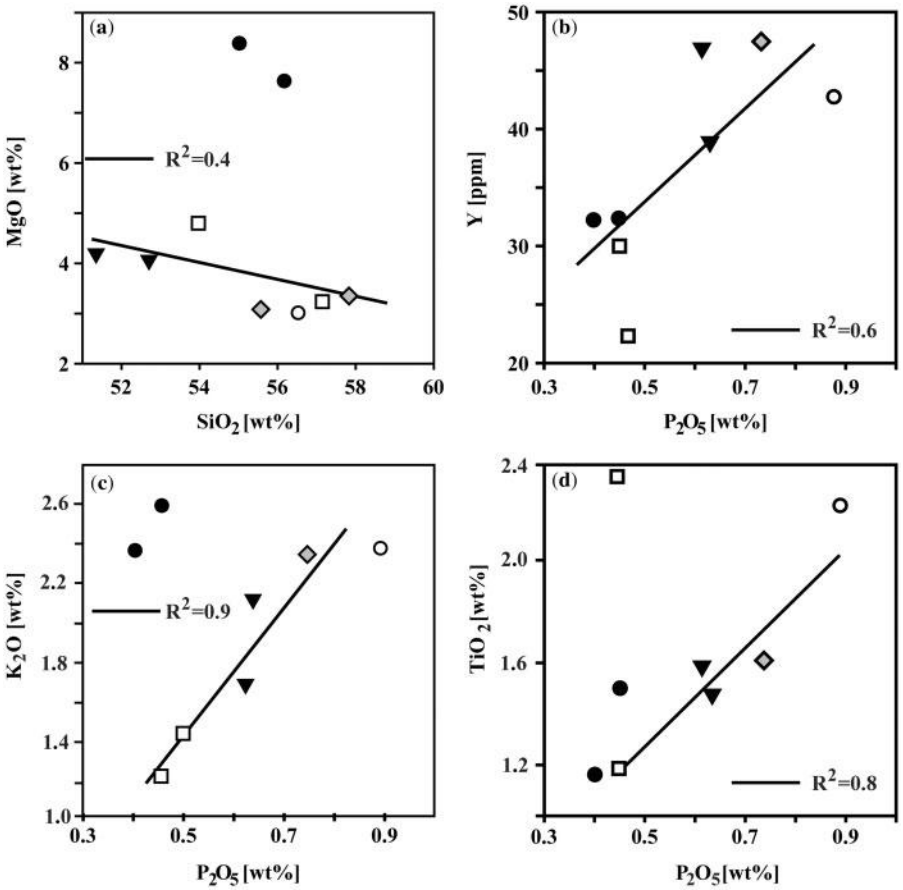

Fig. 5. (a–d) Selected major element vs major or trace element diagrams. Symbols as in Fig. 4. R^2 represents the linear regression coefficient of the data excluding high-Mg samples (●).

Table 3: Rb-Sr ages for the various types of the Gęsiniec quartz diorite

Rock	Isochron	Age (Ma)	No. of points	Initial ratio	MSDW	Comments
LPD	WR + biotit + plag	294·0 ± 0·6	5	0·70695 ± 0·0001	10·6	homogeneous plagioclase
LPD	WR + plag	307·0 ± 4·8	4	0·70691 ± 0·00003	1·7	
MD	WR + biotit + plag	296·7 ± 0·7	5	0·70737 ± 0·00008	4·8	heterogeneous plagioclase
LMGD	WR + biotit + plag	294·8 ± 0·6	6	0·70776 ± 0·00006	2·0	homogeneous plagioclase
LMGD	WR + plag	281 ± 26	5	0·70778 ± 0·00007	2·9	
LCGD	WR + biotit + plag	306·7 ± 1·6	17	0·70770 ± 0·00015	136	strongly heterogeneous plagioclase

Errors and mean square weighted deviations were calculated using Isoplot 3.07 (Ludwig, 2004). The errors used to calculate ages were 0·1% for $^{87}Rb/^{86}Sr$ and 0·007% for $^{87}Sr/^{86}Sr$ based on replicate analyses of standards. WR, whole-rock.

whereas Zone B and Zone C occur only in smaller grains. This is in agreement with the larger grains representing sections through crystal centers, whereas the smaller grains represent random cuts through the outer parts of plagioclase crystals or later stages of plagioclase growth.

Sr isotope composition, trace element and orthoclase content in plagioclase

Variations in the initial Sr isotopic composition of plagioclase are presented in Fig. 8 and Table 6. Where possible, we attempted to sample discrete zones formed before and

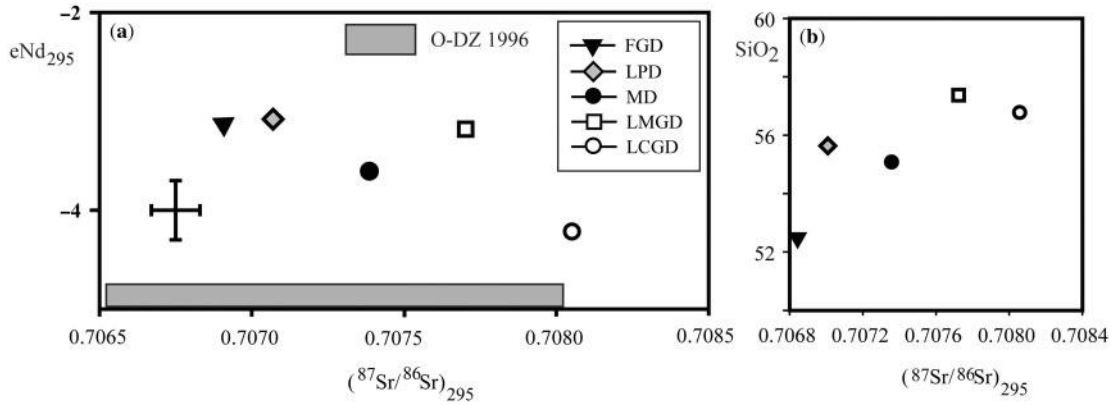

Fig. 6. (a) $^{87}Sr/^{86}Sr_{295}$ vs ε_{Nd295} for the Gęsiniec samples. Grey field represents the range of Sr isotopic composition in the Gęsiniec Intrusion reported by Oberc-Dziedzic *et al.* (1996) recalculated to $^{87}Sr/^{86}Sr_{295}$, (b) $^{87}Sr/^{86}Sr_{295}$ vs SiO_2 (whole-rock composition) for the Gęsiniec samples.

Table 4: Sr and Nd isotopic composition

Sample	$^{87}Sr/^{86}Sr_{295}$	ε_{Nd295}	$^{87}Sr/^{86}Sr$	2 SE%	Rb (ppm)	Sr (ppm)	$^{87}Rb/^{86}Sr$	$^{143}Nd/^{144}Nd$	Sm (ppm)	Nd (ppm)	$^{147}Sm/^{144}Nd$
FGD	0·70690	−3·17	0·70941	0·0009	69·7	337·4	0·5979	0·51232	10·1	53·0	0·115135
LPD	0·70705	−3·07	0·71077	0·0011	93·0	303·9	0·8854	0·51233	10·2	52·2	0·119043
MD	0·70737	−3·61	0·71285	0·0013	90·6	200·9	1·3054	0·51230	7·1	37·7	0·114940
LMGD	0·70770	−3·17	0·70941	0·0011	48·6	328·1	0·4286	0·51232	5·1	26·2	0·118041
LCGD	0·70804	−4·22	0·71217	0·0012	100·0	293·5	0·9837	0·51227	9·2	47·7	0·117476
biotite LPD			0·921886	0·0016	351·0	20·2	51·3807				
biotite MD			0·843736	0·0047	305·5	27·7	32·301				
biotite LMGD			0·831122	0·001	324·0	32·3	29·4057				
biotite LCGD			0·835479	0·0019	387·9	38·8	29·2762				

Multiple analyses of SRM987 and JM Nd at Copenhagen University standard yielded values of $^{87}Sr/^{86}Sr = 0{\cdot}710233 \pm 28$ ($n = 11$), $^{87}Rb/^{85}Rb = 0{\cdot}3856 \pm 6$ ($n = 17$) and $^{143}Nd/^{144}Nd = 0{\cdot}511115 \pm 3$ ($n = 6$), all errors 2σ. Rb, Sr, Sm and Nd concentration were measured by isotope dilution.

Table 5: Morphology and An content in plagioclase

Zonation:	No. samples/grains analysed	Zone A, An mol% unzoned	Zone A, size (μm)	Zone A-B boundary	Zone B normally zoned	Zone B-C boundary Embayed	Zone C
LPD	4/15/4	—	—	—	65–41	1 or more embayments resorbing entire grain interior	23–47
MD	4/21/5	59–64	~200	rounded	69–26 (70–72; spike at boundary)	2–3 embayments per grain	20–48
LMGD	3/14/4	—	—	—	58–40	1 or more embayments resorbing entire grain interior	29–47
LCGD	2/15/7	58–66	~800	slightly rounded	64–38 (67–72; spike at boundary)	2–3 embayments per grain	21–45
MCGD-x	1/4/3	—	—	—	54–43	2–3 embayments per grain	28–47

Column 2 gives the number of samples and plagioclase grains analyzed for An content and by LA-ICPMS (first, second and third number, respectively). —, zone is absent from the lithology.

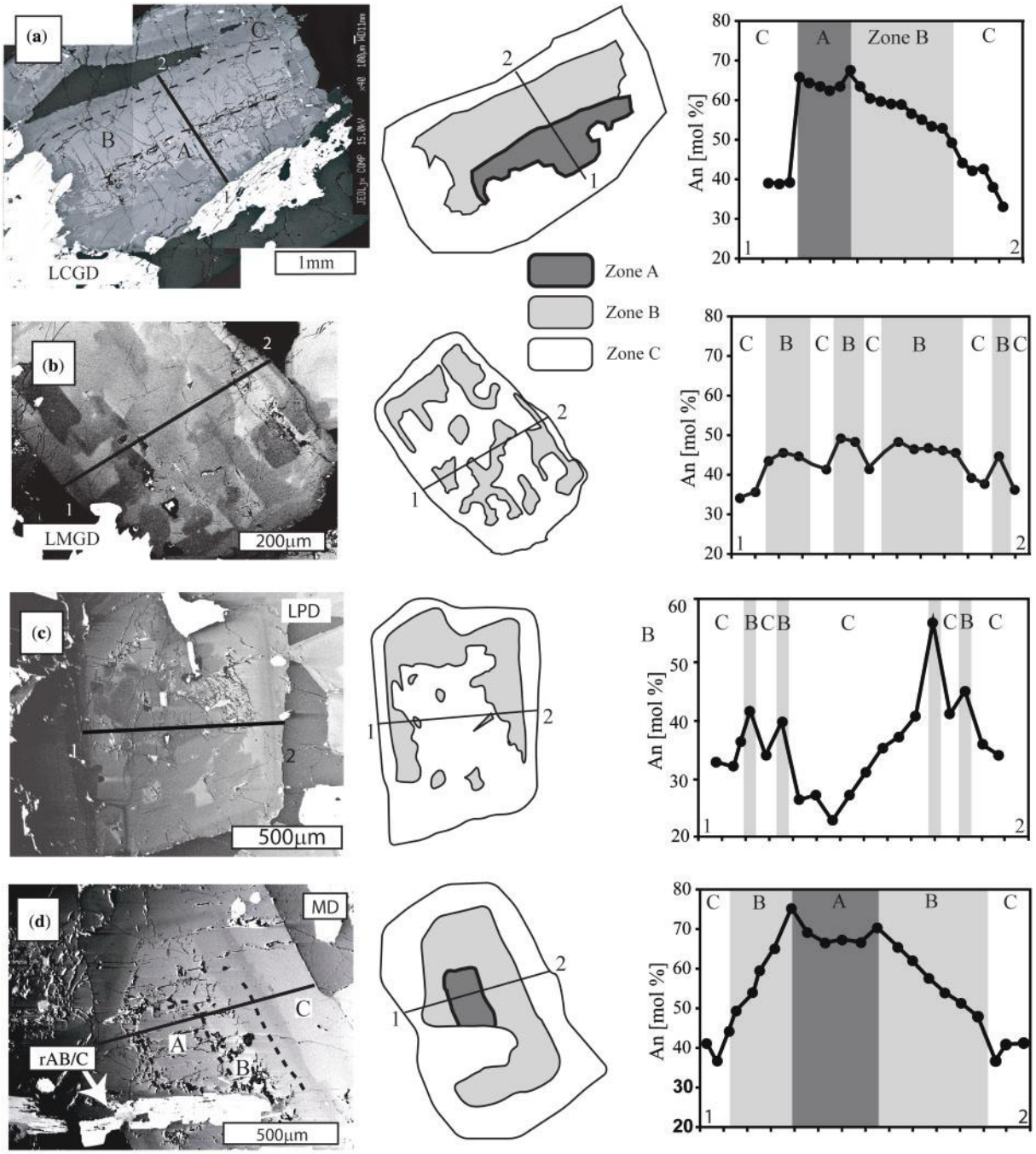

Fig. 7. Back-scattered electron (BSE) images of representative plagioclase crystals with schematic sketch and corresponding An profiles measured by microprobe. (a) Plagioclase from LCGD, showing an asymmetric zoning profile; (b) plagioclase from LMGD, showing complex patchy zoned interior; (c) plagioclase from LPD, showing strong resorption of the grain interior; (d) plagioclase from MD, showing two resorption surfaces: a rounded one between Zones A and B and an embayed one between Zones B and C but cutting into Zone A as well.

after resorption. However, in samples where the grain size was too small, or the resorption geometry too complex, to achieve this goal we sampled whole grains with different proportions of Zone B to Zone C, such that if there is a contrast in Sr isotope composition over the resorption surface, we would obtain a correlation between the isotopic composition and the relative proportion of Zone B and Zone C sampled (Table 6). FGD samples were excluded because the grain size was too small for meaningful analyses of Sr isotopes and trace elements to be made.

The extent of initial Sr isotopic heterogeneity observed in single plagioclase grains and between grains differs

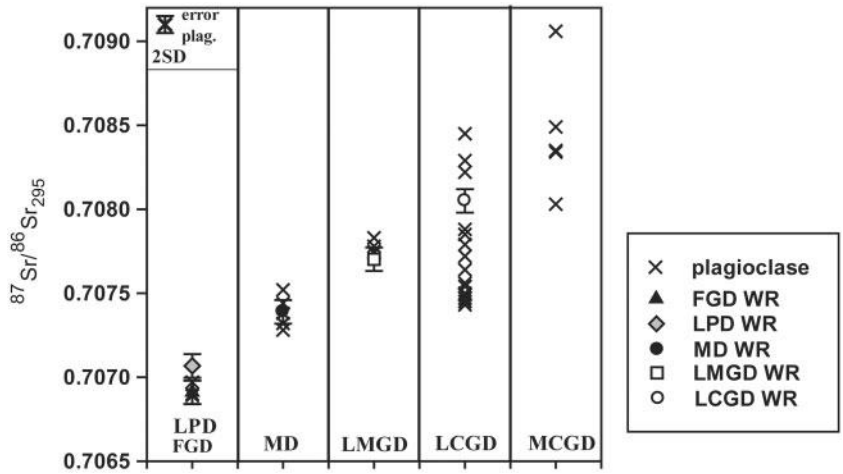

Fig. 8. Range of $^{87}Sr/^{86}Sr_{295}$ whole-rock and plagioclase compositions (×) for the Gęsiniec rock types.

significantly between quartz diorite types from ~150 to ~1500 ppm (Fig. 8, Table 6). In two of the quartz diorite types there is almost no difference in isotopic composition (LPD and LMGD, Tables 6 and 7). Other lithologies (LCGD, MD and MCGD-x) exhibit variation in Sr isotope composition within high-An interiors (Zone A + B) or from grain to grain, but only rarely over the strongly embayed Zone A + B–Zone C resorption surface (Table 6, Fig. 9). The Sr isotopic variability in Zone A and B from grain to grain in one sample is probably due to sampling of strongly isotopically heterogeneous material. In the quartz diorite with the largest grain size (LCGD) the maximum variation in Sr isotope composition occurs before the resorption, within the high-An interiors. Initial $^{87}Sr/^{86}Sr$ increases, probably across the Zone A–Zone B boundary; Zone A yields consistent, similar $^{87}Sr/^{86}Sr$, whereas Zone B is always more radiogenic and more variable (Fig. 9a, Table 7). The Sr isotope composition of Zone C is either similar to (Fig. 9b–e) or less radiogenic than (Fig. 9a) that of the high-An plagioclase in contact with Zone C (because of the complex geometry of the resorption surface, Zone C may be in direct contact with either Zone A or Zone B; Fig. 9).

Additional information is provided by the trace element concentrations in plagioclase (Supplementary Data, Appendix 2). The trace and major element compositions of Zone A have the potential to preserve information about the parental magma composition. The composition of Zone A plagioclase partially overlaps between the quartz diorite types (MD, LCGD) and is characterized by lower Or%, Sr, Ba and LREE compared with Zone B (Table 7). The differences in Zone A composition between LCGD and MD types (e.g. LREE and Pb; Fig. 10) are most probably due to the small size of Zone A in MD (Table 5) compared with the sampling size of the laser; this means that, in many instances, analyses may represent material from several zones (e.g. Zones A + B or B + C).

As Zone B and Zone C plagioclase with similar ranges of An content occur in all quartz diorite types their compositions can be compared between the types. Such a direct comparison of plagioclase compositions at a given An content is justified because trace element partitioning depends predominantly on An content (e.g. Bindeman *et al.*, 1998). A compositional comparison of Zone B in the various quartz diorite types is presented in Table 6 and Fig. 11. For two quartz diorite types (LPD, LMGD) it was difficult to sample Zone B separately from Zone C, as embayments in those types are abundant and closely spaced (e.g. Fig. 7b and c) and mixing of zones during laser ablation was unavoidable. In particular, analyses that intended to sample plagioclase with the highest An content are most probably mixtures of both zones.

The largest variations in Zone B composition between quartz diorite types are observed in Or% (mol % orthoclase) and Pb (Fig. 11). Two groups can be distinguished: (1) high Pb and low Or%, including two quartz diorite types (MD, LMGD); (2) low Pb and high Or%, also including two quartz diorite types (LCGD, MCGD-x, Table 7, Fig. 11). LPD plots between these two groups for Pb and has Or contents similar to the latter group. Sr and LREE concentrations partly overlap between all quartz diorite types; however, Zone B in LMGD has the lowest concentrations, whereas Zone B plagioclase grains from MD and LPD have the highest (Table 7, Fig. 11).

Generally, we observe continuous changes in most trace element contents coupled with decreases in An content in Zone B and C (Fig. 11). However, no abrupt change in trace element composition is observed between Zone B and Zone C (Fig. 11). A large compositional change may be observed when previously crystallized Zone A or B is deeply cut by an embayment. However, we stress that this does not represent the record of any significant change in the surrounding magma composition during crystallization but is an artefact of the resorption surface geometry.

Table 6: Rb-Sr isotopic data for plagioclase from the Gęsiniec Intrusion

Grain no.	Zone*	No.	Rb (ppm)	Sr (ppm)	$^{87}Rb/^{86}Sr$	2σ	$^{87}Sr/^{86}Sr$	2σ	$^{87}Sr/^{86}Sr$ at 295 Ma
LPD									
	whole C>B	53	18·9	1036·5	0·0526	1·0E – 04	0·707124	1·2E – 05	0·7069
	whole B>C	58	7·9	826·0	0·0277	2·5E – 05	0·707005	8·5E – 06	0·70689
	3 grains B>C	59	31·2	744·5	0·1211	1·1E – 04	0·707473	6·4E – 06	0·70697
MD									
	whole	51	17·2	951·8	0·0523	3·7E – 05	0·707594	7·8E – 06	0·70738
	whole	54	5·5	682·1	0·0235	1·5E – 05	0·70754	9·9E – 06	0·70744
d20-75	inner part	55	6·8	993·9	0·0199	1·9E – 05	0·7074	1·3E – 05	0·70732
d20-75	outer part	60	40·0	800·2	0·1445	1·6E – 04	0·707886	1·3E – 05	0·70728
	whole	61	17·1	368·9	0·1344	1·4E – 04	0·708077	1·8E – 05	0·70752
LMGD									
	whole	32	4·0	522·3	0·0221	1·3E – 05	0·707832	9·9E – 06	0·70774
	whole	33	1·1	503·7	0·0065	4·1E – 06	0·707776	1·1E – 05	0·70775
	whole	50	2·2	610·0	0·0150	7·2E – 06	0·707876	8·5E – 06	0·70783
	4 grains	39	10·9	611·0	0·0514	3·8E – 05	0·707998	1·3E – 05	0·70778
LCGD									
d19-1-2	C	5	2·0	389·7	0·0145	3·5E – 05	0·707776	1·7E – 05	0·70772
d19-2-1	A	10	3·5	787·1	0·0130	1·0E – 05	0·707557	9·2E – 06	0·7075
d19-2-2	B, c	12	4·2	739·9	0·0165	1·7E – 05	0·707629	7·1E – 06	0·70756
d19-2-2	A	7	5·7	939·6	0·0174	1·8E – 05	0·707518	8·5E – 06	0·70745
d19-1-1a	B	36	2·4	529·3	0·0133	9·2E – 06	0·707847	2·1E – 05	0·70779
d35-3-6	A	22	5·8	979·4	0·0170	1·5E – 05	0·7075	9·9E – 06	0·70743
d35-3-6	B, c	30	8·9	1023·63	0·0252	3·2E – 05	0·707745	2·6E – 05	0·70764
d35-3-6	C	29	3·0	796·6	0·0109	7·4E – 06	0·707685	8·5E – 06	0·70764
d35-3-3	A	20	5·8	562·6	0·0300	5·0E – 05	0·707669	2·2E – 05	0·70754
d35-3-3	B, c	27	1·6	516·2	0·0091	8·4E – 06	0·708332	9·9E – 06	0·70829
d35-3-3	C	28	2·0	564·1	0·0102	6·2E – 06	0·707918	8·5E – 06	0·70788
d35-4-1	A, c	34	2·7	584·5	0·0134	1·1E – 05	0·707529	9·9E – 06	0·70747
d35-4-1	C, b	35	2·5	746·4	0·0098	7·4E – 06	0·707528	1·3E – 05	0·70749
d35-4-4	C	11	1·1	700·2	0·0046	1·1E – 05	0·707866	9·2E – 06	0·70785
d35-2a-1	B, c	56	8·8	754·5	0·0338	3·7E – 05	0·708594	9·9E – 06	0·70822
d35-2a-1	B, a	57	1·7	1041·5	0·0047	6·6E – 06	0·708239	2·1E – 05	0·70845
MCGD-x									
d23-1-5	B	21	2·8	513·4	0·0156	8·1E – 06	0·70856	8·5E – 06	0·70849
d23-1-5	B, c	23	0·9	452·5	0·0055	6·9E – 06	0·708377	9·9E – 06	0·70835
d23-1-5	C	24	1·7	578·1	0·0083	5·1E – 06	0·708371	9·9E – 06	0·70834
d23-1-6	B	25	1·2	630·9	0·0056	9·0E – 06	0·709085	1·3E – 05	0·70906
d23-1-1	whole	26	0·5	260·9	0·0051	2·8E – 06	0·708051	1·3E – 05	0·70803

The error (2σ) on a single measurement of $^{87}Sr/^{86}Sr_{295}$ ratio in plagioclase is ±0·00005 and represents propagated internal error on $^{87}Sr/^{86}Sr$ and $^{87}Rb/^{85}Rb$ external error and age.

*As the drill size was relatively large, some samples represent material from several zones, as indicated in the 'Zone' column; upper case letters refer to the Zone that contributed most to the analysis; 'whole' means that whole grain area was sampled. Because of their relatively small grain size compared with the size of the drill bit available, only one micro-drill per plagioclase crystal was collected in LPD and LMGD subtypes, whereas it was possible to collect up to three samples per crystal from the LCGD and MCGD-x plagioclase grains and up to two samples in the MD plagioclase.

Table 7: Summary of Sr isotope, trace element (TE) and minor element (ME) composition of plagioclase

Sr isotopes	Zone A; Sr isotopes	Zone A; ME, TE	Zone A–Zone B boundary; ME, TE	Zone B; Sr isotopes, ME, TE	Zone C; Sr isotopes, ME, TE
LPD					
homogeneous 0·70694 ± 5	—	—	—	High Or (max. >1·4%) High Sr (720–1050 ppm) Pb (5–16 ppm) LREE–La (9–17 ppm) Ba (124–242 ppm) Mn (13–26 ppm) Ti (27–211 ppm)	Range of concentrations for Or (0·5–2·4%). Continuous decrease in most TE with An
MD					
heterogeneous 0·70728 ± 5–0·70752 ± 5	Not characterized because of small size	Or 0·1–0·6% Sr 662–748 ± 7 ppm Pb 7·8–12 ± 7·8 ppm Ba 69–137 ± 3 ppm La 8·1–13·7 ± 1·6 ppm	Abrupt increase in Pb, Sr, LREE	$^{87}Sr/^{86}Sr_i$ n.d. Low Or (max. <1%) High Sr (884–1050 ppm) High Pb (9–27 ppm) High LREE–La (14–30 ppm) Ba (110–190 ppm) Mn (10–35 ppm) Ti (50–215 ppm)	$^{87}Sr/^{86}Sr_i$ n.d. Decrease in Or to 0·2%. Constant Sr content. Range of other trace elements
LMGD					
homogeneous 0·70778 ± 5	—	—	—	Low Or (max. <1·6%) Low Sr (559–764 ppm) High Pb (6–26 ppm) Low LREE–La (6–17 ppm) Ba (92–190 ppm) Low Mn (5–25 ppm) Low Ti (12–180 ppm)	Decrease in Or to 0·3%. Continuous decrease in most TE with An
LCGD					
heterogeneous 0·70743 ± 5–0·70845 ± 5	homogeneous 0·70743 ± 5–0·70750 ± 5	Or 0·3–1·2% Sr 620–694 ± 7 ppm Pb 4·8–5·5 ± 7·8 ppm Ba 77–89 ± 3 ppm La 5·2–8·3 ± 1·6 ppm	Continuous transition	$^{87}Sr/^{86}Sr_i$ 0·70756–0·70845 High Or (max. >1·5%) Sr 731–970 ppm Low Pb (5–15 ppm) La (7–19 ppm) Range of Ba (81–304 ppm) Mn (15–45 ppm) Ti (70–160 ppm)	$^{87}Sr/^{86}Sr_i$ 0·70749–0·70788. Range of concentrations for Or (0·4–2·6%) and trace elements. Continuous decrease in most TE with An
MCGD					
heterogeneous 0·70803 ± 5–0·70906 ± 5	—	—	—	$^{87}Sr/^{86}Sr_i$ 0·70835–0·70906 High Or (max. >2%) Sr (648–798 ppm) Pb (4–13 ppm) La (11–20 ppm) Range of Ba (178–321 ppm) Mn (17–23 ppm) Ti (120–160 ppm)	$^{87}Sr/^{86}Sr_i$ 0·70834. Range of Or (0·7–2·2%) and other trace elements. Continuous decrease in most TE with An

—, zone is absent from the lithology; n.d., not determined separately for the zone because of small size.

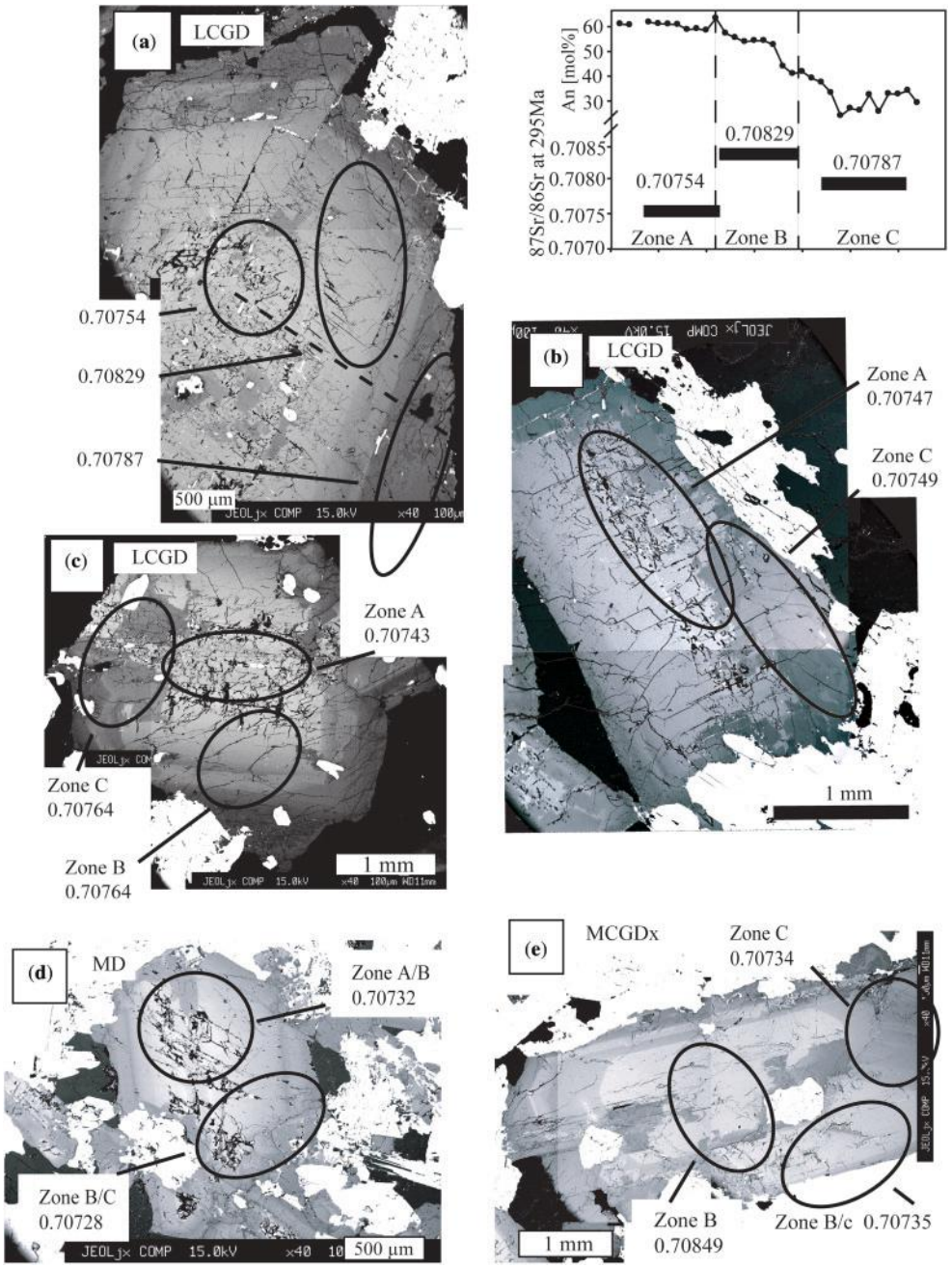

Fig. 9. Examples of plagioclase grains from Gęsiniec quartz diorite. Circles in the BSE images outline the areas sampled for Sr isotope composition; the numbers corresponding to $^{87}Sr/^{86}Sr_{295}$ ratios and the zone from which most of the material was probably sampled are given for each microdrill. Anorthite and $^{87}Sr/^{86}Sr_{295}$ traverses correspond to (a).

DISCUSSION

Significance of resorption in plagioclase

The morphology and composition of plagioclase has been widely used to identify changes in magma crystallization conditions and composition (e.g. Vance, 1965; Smith & Brown, 1988; Ginibre *et al.*, 2007). Recent advances in analytical methods have allowed tracking of isotopic and trace element changes across resorption boundaries, and these have been correlated with open-system processes in both plutonic and sub-volcanic magma systems (Tepley & Davidson, 2003; Davidson *et al.*, 2007; Gagnevin *et al.*, 2007; Ginibre *et al.*, 2007). Embayed resorption, patchy zonation and abrupt decreases in An content across resorption surfaces in plagioclase are common features in many

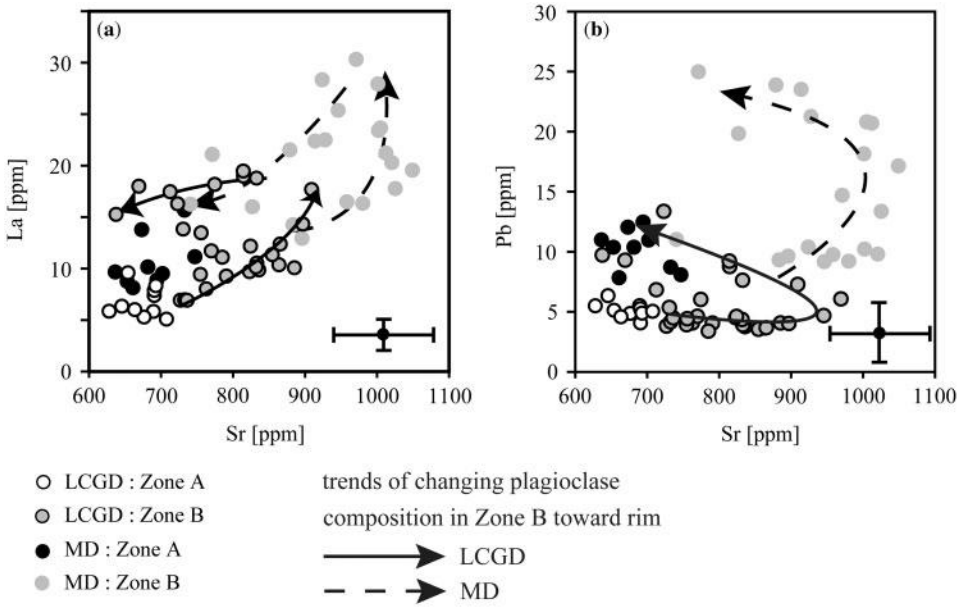

Fig. 10. (a, b) Comparison between trace element composition of Zone A and Zone B plagioclase in MD and LCGD types.

dioritic–tonalitic rocks (e.g. Janoušek *et al.*, 2004; Christofides *et al.*, 2007), including the Gęsiniec Intrusion, and are often assumed to reflect magma mixing (e.g. Hibbard, 1981). The general occurrence of dioritic enclaves containing such plagioclase grains in granodioritic and granitic batholiths seems to corroborate the magma-mixing model (e.g. Elburg, 1996). However, if the extensive, embayed resorption of plagioclase (i.e. between Zone A or Zone B and Zone C, depending on the geometry of the embayed resorption surface; Fig. 9) in rocks from the Gęsiniec Intrusion was due to magma mixing we would expect a consistent change in Sr isotopic composition across this resoption boundary, which is not the case. In fact, in two quartz diorite types (LPD, LMGD) plagioclase is isotopically homogeneous, arguing against any open-system processes during quartz diorite magma crystallization and resorption. Moreover, plagioclase grains from quartz diorites with the most radiogenic Sr isotope composition (LCGD, MCGD-x) are not characterized by any consistent change across the resorbed, embayed boundary. The Sr isotopic compositions recorded after resorption are similar to, or lower than, the compositions of the plagioclase in immediate contact with Zone C. This is consistent with Zone C Sr isotopic compositions being mainly affected by the composition of the high-An core (Zone A + B). Because the cores in some quartz diorite types are isotopically heterogeneous their resorption results in a similarly isotopically heterogeneous Zone C. For example, if Zone B was preferentially resorbed, Zone C crystallized within the embayments would have Sr isotopic compositions typical of Zone B plagioclase (Fig. 9b, d and e). In contrast, if Zone A was resorbed, Zone C would have Sr isotopic compositions typical of Zone A or intermediate between Zone A and B (Fig. 9a and c). Such a strong dependence of Zone C isotopic composition on the composition of the resorbed interior requires that the melt trapped in the embayments did not equilibrate with the surrounding melt and preserved the isotopic composition of the plagioclase that was resorbed. As equilibration of Sr isotopic compositions in melts is very rapid (Lesher, 1994) the preservation of such gradients would require the presence of some sort of a barrier between the melt in the embayments and the melt outside to prevent equilibration and/or very rapid crystallization after the resorption. An alternative explanation is that differences in Sr isotopic compositions between Zone C in different plagioclase grains (Fig. 9) could be an artefact of imperfectly constrained sampling in the *z* direction that could include plagioclase from other zones as a result of the complex Zone C morphology. However, much better resolution of both the isotopic and trace element composition of plagioclase in the embayments is required to constrain the presence of compositional heterogeneities between embayments in different grains, their extent and possible impact on timescales of diffusional equilibration. There is no evidence for Zone C crystallization from an isotopically distinct magma compared with that from which the high-An cores (Zone B) crystallized. Differences in Sr isotopic composition of Zone C from grain to grain in isotopically heterogeneous quartz diorite types (MD, LCGD, MCGD) are a direct result of isotopic heterogeneity in high-An interiors (Zone A + B).

The main conclusion from these observations is that the resorption event between Zone A + B and Zone C and the

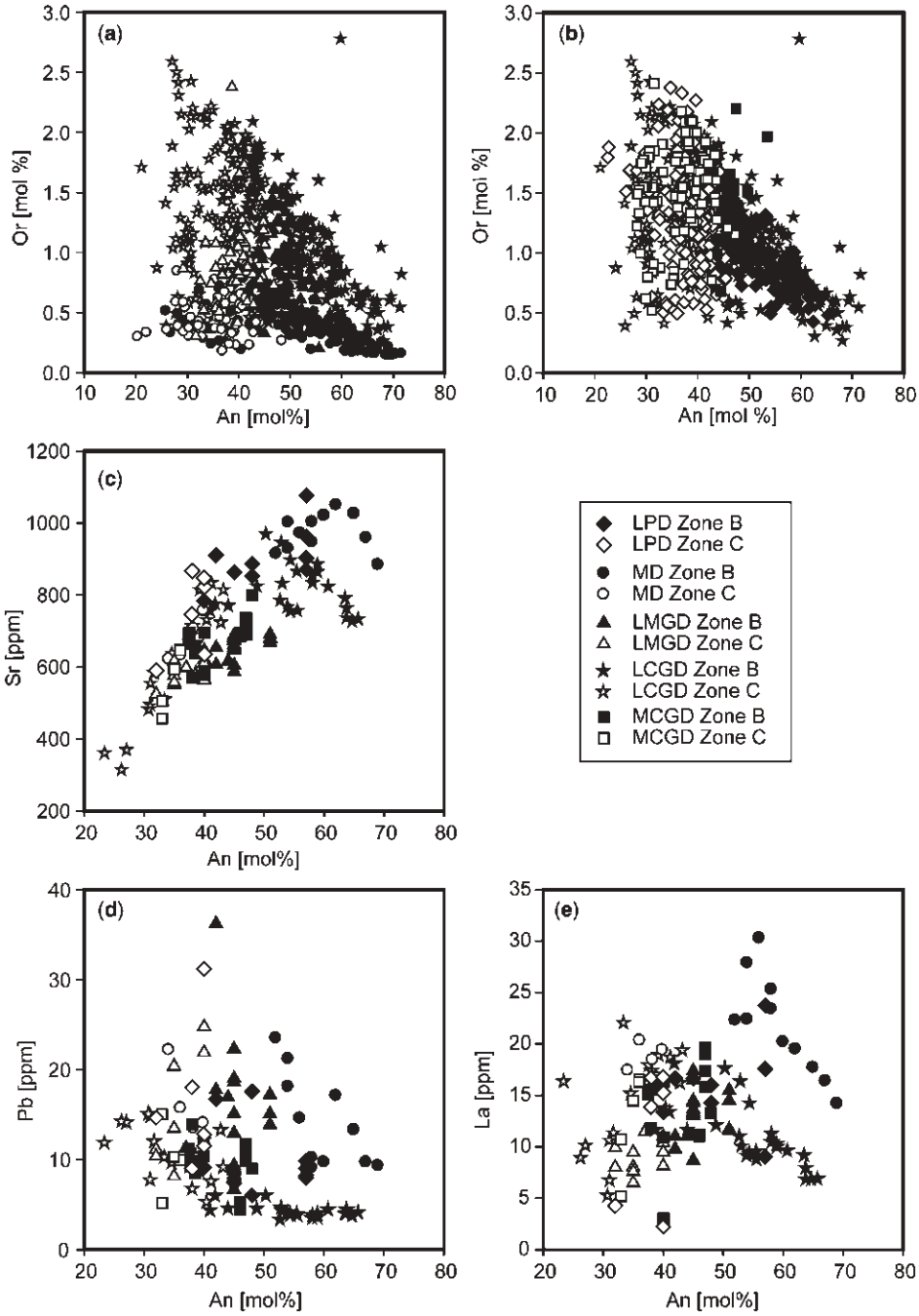

Fig. 11. (a–e) Anorthite vs trace elements plots for the various types of Gęsiniec quartz diorites.

development of patchy zonation and strongly embayed high-An cores could not be due to mixing of two isotopically contrasting magmas (e.g. the often proposed mixing of felsic and mafic magmas; Hibbard, 1981), nor be due to any other open-system process. The record of open-system processes is preserved only within the high-An cores of plagioclase from three quartz diorite types (MD, LCGD, MCGD) and, therefore, open-system processes must have taken place before the cores were resorbed and were not a direct cause of the resorption. Therefore, we need to ask: what triggered the resorption? Apart from a significant shift in magma composition, which often accompanies open-system processes, resorption of plagioclase may be induced by an increase in temperature or a reduction in pressure. However, the characteristic embayed morphology of the resorption surface observed between Zones

A + B and Zone C in plagioclase at Gęsiniec has not been observed in experimental studies in which increased temperature or changes in melt composition were the cause of resorption of plagioclase (Tsuchiyama, 1985; Johannes *et al.*, 1994; Nakamura & Shimakita, 1998). Instead, only the decompression experiments of Nelson & Montana (1992) produced embayed crystals with partly preserved euhedral outer surfaces similar to those observed in the Gęsiniec plagioclase. Thus, we suggest that the resorption effects observed could be induced by decompression. This conclusion is supported by the lack of any dramatic change in the An, Or and trace element composition (Fig. 11) or Sr isotope composition (Fig. 9) of the plagioclase before and after resorption.

Rapid movement of an ascending, crystal-rich magma could be responsible for the fragmentation of plagioclase crystals that, in turn, leads to non-symmetrical zonation patterns within individual grains. Similar features observed in plagioclase from other dioritic–tonalitic (e.g. Vance, 1965; Blundy & Shimizu, 1991; Janoušek *et al.*, 2004) and more felsic intrusions (Pietranik *et al.*, 2006) could also be decompression related. Rapid magma ascent in dykes and the importance of decompression in magma evolution models is currently widely accepted (e.g. Petford *et al.*, 2000; Annen *et al.*, 2006; Kemp *et al.*, 2007; Ginibre *et al.*, 2007). Our data provide additional evidence that such rapid decompression might often be the case. Attributing the embayed resorption to decompression has one additional implication; plagioclase that crystallized before the decompression-induced resorption (Zones A and/or B) provides an unparalleled opportunity to study processes that happened before magma emplacement close to the surface, probably somewhere in the lower crust. We emphasize that this early crystallization stage was characterized by open-system processes, at least in the quartz diorite types that preserve evidence of isotopic heterogeneity within plagioclase crystals, whereas there is no evidence that open-system processes acted during the later formation of strongly embayed resorption surfaces and patchy zonation. Below we discuss the plagioclase record from Zone A and Zone B together with whole-rock geochemistry to unravel the early stage of magma differentiation.

Dioritic–tonalitic magma evolution: comparing the plagioclase and whole-rock records

The Gęsiniec Intrusion is interpreted as a cross-section through a composite dyke (Oberc-Dziedzic, 1999*b*) that was probably assembled from several distinct ascending magma pulses that froze on their way to the surface. Freezing of magma in a conduit upon ascent, probably caused by crossing of the water-saturated solidus (e.g. Johannes & Holtz, 1996), preserves the early formed textures and compositional relationships generated at depth. Similar relationships may be lost from the plagioclase record if the magma underwent an evolutionary stage in a sub-volcanic magma chamber where several magma pulses assembled and mixed before complete crystallization or eruption. Therefore, by studying plagioclase in small intrusions with evidence of very limited post-emplacement interaction between several distinct magmas has the potential to improve our understanding of magmatic differentiation processes in the lower crust. Our study employs this approach to understand the evolution of dioritic–tonalitic magmas that are often thought to represent a link between mafic and felsic magmatism. However, as shown above, the record of mafic and felsic magma interaction is not preserved across strongly embayed resorption boundaries in plagioclase between Zones A + B and Zone C, which we interpret to be due to closed-system resorption. We argue that the processes that caused the isotopic variability in the Gęsiniec quartz diorites happened before magma emplacement and are, therefore, potentially recorded within the high-An cores of plagioclase (Zone A + B) as well as in the whole-rock geochemistry.

The general view of magmatism in orogenic settings involves intrusion of mantle-derived magmas into the lower crust, remelting of the lower crust (underplated material and pre-existing older crust) to produce granitic to dioritic magmas, and evolution of both mantle- and crustal-derived magmas by fractional crystallization and/or magma–crust interaction (e.g. Annen *et al.*, 2006; Kemp *et al.*, 2007). Evidence for interaction between mantle- and crustal-derived magmas is preserved, for example, in the variability of Hf isotope compositions in zircons from I-type granites in Lachlan Fold Belt of Australia (Kemp *et al.*, 2007). Dioritic to tonalitic intrusions are globally much less voluminous than granitic batholiths and mafic layered intrusions; however, their typically intermediate isotopic compositions between mantle- and crustal-derived magmas may suggest that they also record an important interaction process (Fig. 12).

The SiO_2 contents of the dioritic–tonalitic rocks in the Gęsiniec Intrusion seem to be too low, and Mg contents too high, to support crustal derivation of the Gęsiniec magmas unless temperatures of >1000°C were reached (Rapp & Watson, 1995). Conversely, the initial Sr isotopic compositions of ~0·707 and ε_{Nd} of ~–3 are outside the range of typical mantle compositions. Therefore, hybridization between mantle- and crustal-derived magmas is a reasonable hypothesis for the ultimate source of the dioritic–tonalitic magmas and is supported by AFC or magma-mixing modelling in the Gęsiniec (Fig. 12) and many other intrusions (e.g. Janoušek *et al.*, 2000; Pinarelli *et al.*, 2002). However, the melting of relatively old basaltic crust cannot be excluded, as small amounts of dioritic melt can be produced after hydrous mantle-derived magmas intrude amphibolitic lower crust (Annen *et al.*, 2006). Is it possible

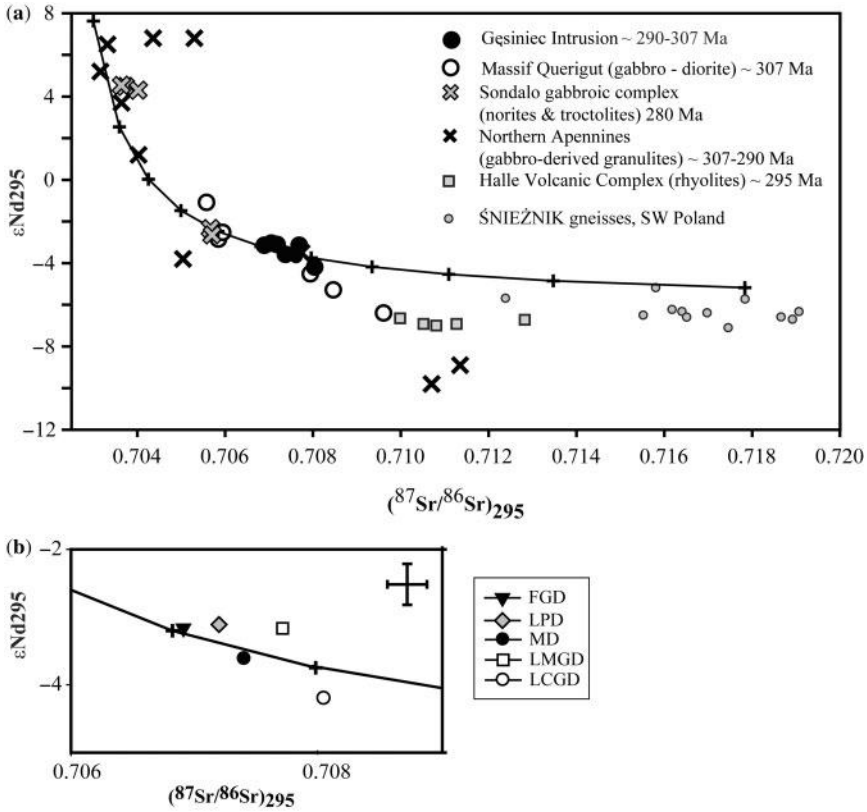

Fig. 12. (a) Variation of initial $^{87}Sr/^{86}Sr$ vs initial ε_{Nd} in plutonic and volcanic rocks of Late Carboniferous–Permian age (307–290 Ma). Continuous line represents magma bulk mixing between the most mafic, mantle-derived, Variscan igneous rocks at 290 Ma and Variscan basement at 290 Ma. Parameters for the mixing calculations are: for the mafic end-member: $\varepsilon_{Nd} = 7{\cdot}6$, $^{87}Sr/^{86}Sr_{290} = 0{\cdot}703$, Nd 10 ppm, Sr 400 ppm (Nd and Sr are average values for mantle-derived basaltic magmas. from the GeoRoc database); for the felsic end-member $\varepsilon_{Nd} = -7{\cdot}0$, $^{87}Sr/^{86}Sr_{290} = 0{\cdot}718$, Nd 40 ppm, Sr 100 ppm [approximate values for Variscan gneisses at 290 Ma, e.g. Śnieżnik gneisses (Lange *et al.*, 2005) and S-type granites from SW Poland, J. Białek, unpublished data]. Igneous rock data are for tonalitic to gabbroic rocks from the Querigut Massif (Roberts *et al.*, 2000), Sondalo gabbroic complex (Tribuzio *et al.*, 1999), gabbro-derived granulites from Northern Apennines (Montanini & Tribuzio, 2001) and felsic volcanic rocks from Halle Volcanic Complex (Romer *et al.*, 2001). (b) Enlarged diagram of bulk mixing modeling shown for Gęsiniec rocks only.

to distinguish between those two magma sources and evolution paths?

A first approach to solve this problem should be to explain the range of isotopic compositions observed in the dioritic–tonalitic rocks, as it is probable that the magmatic differentiation process that produced the intermediate isotopic compositions (i.e. plotting between the mantle and the old crust in Fig. 12) of the least evolved rocks (FGD, LPD) might be also responsible for the within-suite isotopic differences. That the isotopic differences between the quartz diorite magma types were probably already developed before their final emplacement is consistent with the crystallization of isotopically heterogeneous plagioclase cores (Zone A + B) and the lack of evidence for open-system processes during Zone C crystallization. The generally similar patterns on multi-element variation diagrams and similar trace element ratios suggest that the dioritic–tonalitic magmas in the Gęsiniec Intrusion were related and that there is no reason to believe that the parental magmas were derived from two or more compositionally distinct sources. Although compositional heterogeneities in the mantle or crustal source cannot be excluded, as some differences (e.g. in Th and U whole-rock contents) between types are observed (Table 2), the general similarities in whole-rock composition justify the assumption that the parental magmas are similar. In the simplest case scenario a single continuous hybridization process between two end-members would produce a range of isotopic and major and trace element compositions. However, no clear correlation between whole-rock Sr isotopic and major or trace element composition is observed in the Gęsiniec rocks (Fig. 6), or other dioritic–tonalitic suites (e.g. Roberts *et al.*, 2000). This is perhaps to be expected for two reasons: (1) plutonic rocks are prone to late-stage melt removal that may significantly change the trace element composition of the whole-rock; (2) it has been shown that hybrid rocks can actually be mixtures of isotopically and compositionally distinct crystal cargoes

(e.g. Waight *et al.*, 2000; Davidson *et al.*, 2007; Kemp *et al.*, 2007; Beard, 2008) and therefore they may not exhibit the simple correlations typical of more simple melt-mixing models.

The best approach to understand the isotopic diversity of dioritic–tonalitic rocks is to seek correlations between whole-rock isotopic composition and mineral isotopic and trace element compositions. Positive correlations between whole-rock Sr isotopic composition and the range of isotopic heterogeneity as well as the maximum $^{87}Sr/^{86}Sr_{295}$ in the Gęsiniec plagioclase (Fig. 8) appears to support a simple model of fractional crystallization of a low $^{87}Sr/^{86}Sr_{295}$ magma that becomes progressively contaminated by a more radiogenic crustal component. In earlier, hotter and less viscous magmas, crystals are efficiently removed from the magma and only isotopically homogeneous crystals remain in the magma (timescales of crystal removal by fractional crystallization are shorter than the timescales of contamination). As the magmas become more contaminated they become more viscous, and timescales of contamination overtake those of fractional crystallization and result in the retention of isotopically heterogeneous crystals. However, two lines of evidence do not support this simple model, as follows.

(1) Zone A plagioclase is present in the quartz diorite with the most radiogenic $^{87}Sr/^{86}Sr_{295}$ whole-rock composition (LCGD). Zone A has lower concentrations of many incompatible elements such as LREE, Ba and Sr and lower $^{87}Sr/^{86}Sr_{295}$ ratios than the surrounding Zone B with similar An content (Fig. 10). This suggests that Zone A was formed from both a less fractionated and a less contaminated magma than surrounding Zone B. In contrast, plagioclase from the quartz diorite with the least radiogenic $^{87}Sr/^{86}Sr_{295}$ whole-rock and plagioclase composition (LPD) does not contain Zone A and the trace element composition of Zone B plagioclase is similar to that of Zone B in the LCGD type (Fig. 11), but has lower $^{87}Sr/^{86}Sr_{295}$. Zone A in the LCGD type is slightly resorbed but there is no difference in An% and the concentrations of many trace elements between Zone A and Zone B that might suggest that Zone A was xenocrystic. Therefore, the high $^{87}Sr/^{86}Sr_{295}$ quartz diorite (LCGD) cannot be derived by simple AFC from the low $^{87}Sr/^{86}Sr_{295}$ quartz diorite (LPD). In other words, the LPD type seems to be more fractionated but less or uncontaminated compared to LCGD.

(2) Quartz diorites with intermediate whole-rock $^{87}Sr/^{86}Sr_{295}$ isotopic compositions (MD, LMGD) are also characterized by distinctive minor and trace element patterns in plagioclase, particularly high Pb and low K concentrations in Zone B. Therefore, although one of these quartz diorites has a high Mg, Cr and Ni whole-rock composition (MD) suggesting that it is a cumulate, it could not be a cumulate produced during AFC processes common for all dioritic–tonalitic rocks in the Gęsiniec Intrusion. Thus, although the parental magmas for all the dioritic–tonalitic rocks were compositionally similar and probably derived from a similar source, each quartz diorite magma type appears to have undergone a separate differentiation stage, possibly in a distinct magma chamber in the lower crust.

The quartz diorites with intermediate Sr isotopic compositions (MD, LMGD) are probably related to each other by a common differentiation process, as suggested by the similar high Pb concentrations and low Or% in Zone B plagioclase and certain similarities in whole-rock geochemistry. The high Mg, Cr, Ni quartz diorite (MD) has a whole-rock chemical composition typical of a cumulate of mafic minerals (amphibole and biotite) and records an episode of early resorption of Zone A plagioclase (Fig. 7d). The resorption happened before Zone B crystallization and the resorption surface is rounded and often cut by later decompression-induced resorption effects (Fig. 7d). This early resorption of Zone A plagioclase could be contemporaneous with slight resorption observed in the mafic minerals (Fig. 3c) and could represent contamination by a more evolved magma (as suggested by the increase in Pb, Sr and LREE across the Zone A–Zone B boundary; Table 7). The magma also probably had a different $^{87}Sr/^{86}Sr$ isotopic composition from the parental magma from which the Zone A plagioclase crystallized. However, it is impossible to track whether $^{87}Sr/^{86}Sr$ increases or decreases from Zone A to Zone B because of the small grain size. The resorption surface is rounded and not embayed, similar to those observed following dissolution of plagioclase in disequilibrium conditions (e.g. Tsuchiyama, 1985). Preferential resorption of Zone A plagioclase with only limited evidence for resorption in coexisting hydrous minerals (biotite and amphibole) suggests that the plagioclase was resorbed in a water-rich magma (e.g. Beard & Lofgren, 1991). It is also possible that biotite and amphibole formed by reaction between anhydrous mafic minerals and a water-rich melt. Such resorption could be an effect of magma mixing or, alternatively, partial melting of mafic lower crust induced by intrusion of hydrous basaltic magma (as modelled by Annen *et al.*, 2006). We propose that the cumulate-like quartz diorite (MD) was produced by the partial extraction of the newly formed melt after the early resorption of Zone A plagioclase. A fully extracted melt, which left the resorbed mineral assemblage (strongly resorbed Zone A plagioclase + slightly resorbed mafic minerals) behind would be rich in Ca, Sr and Eu and poor in K, as a result of the stability of biotite and the instability of plagioclase during the resorption. Such a composition is characteristic of the LMGD type, and supports the conclusion that MD and LMGD are related. The important implications of the observed relationships are that (1) an evolved, water-rich melt was involved in the genesis of the intermediate

$^{87}Sr/^{86}Sr_{295}$ quartz diorites and (2) interaction of rocks or magmas with such melts may produce isotopically heterogeneous 'restite'-bearing rocks and isotopically homogeneous 'restite'-free new melts (it would be truly restite only if the process responsible for the resorption was partial melting; in the case of magma mixing the resorbed minerals should be termed pre-mixing assemblage).

The composition of the contaminant involved in the genesis of the high $^{87}Sr/^{86}Sr_{295}$ quartz diorites (LCGD, MCGD-x) must have been different from that in the intermediate $^{87}Sr/^{86}Sr_{295}$ quartz diorites (MD, LMGD), as indicated by the distinct compositions of the Zone B plagioclase (Figs 10 and 11). Despite the quartz diorites with the lowest and the highest $^{87}Sr/^{86}Sr_{295}$ ratios not being related by a common AFC process, similar An and Or contents in Zone B plagioclase in both types suggest that Zone B might represent the same degree of magma differentiation in both quartz diorite types. Therefore, the compositional differences between Zone B in the low and high $^{87}Sr/^{86}Sr_{295}$ quartz diorites could theoretically be the result of the contamination process. Zone B in the plagioclase from the high $^{87}Sr/^{86}Sr_{295}$ quartz diorite (LCGD) has almost the highest $^{87}Sr/^{86}Sr$ ratios observed in the intrusion and slightly lower Sr contents, whereas the concentrations of other trace element overlap with Zone B plagioclase in the low $^{87}Sr/^{86}Sr_{295}$ quartz diorite (LPD), which does not record any open-system contamination process. This would be expected if we are dealing with small amounts of a typical, high $^{87}Sr/^{86}Sr$ crustal contaminant; for example, 10% of a material with $^{87}Sr/^{86}Sr_{295} \sim 0{\cdot}720$. Such a contaminant would also have a low Sr content (typically 50–100 ppm) and thus be in agreement with general AFC modelling between mantle and crust components (Fig. 12). The contamination in LCGD started after Zone A crystallization, as indicated by the homogeneous Sr isotope composition and trace element contents in Zone A (Table 7). It is probable that the onset of contamination and, therefore, change in the physicochemical properties of the melt, triggered the early resorption of Zone A. Overlapping Sr isotope ratios and trace element contents in Zone B plagioclase from LCGD and MCGD-x suggest that these quartz diorite types are also related. MCGD-x could be derived by an AFC process from LCGD, as supported by the lower An content and higher $^{87}Sr/^{86}Sr_{295}$ in Zone B plagioclase in MCGD-x.

Summarizing, the Zone A and Zone B plagioclase and whole-rock composition show that the quartz diorite magmas not only evolved in at least three separate magma chambers but also interacted with at least two different contaminants before final emplacement, formation of embayed resorption surfaces and Zone C crystallization (Fig. 13). This seemingly complex picture of magma evolution is in agreement with other studies worldwide. For example, Kemp *et al.* (2007) showed that dioritic to granitic rocks from the Lachlan Fold Belt contain isotopically heterogeneous zircon crystals that probably formed in separate magma chambers and were mixed before or after ascent into upper crustal magma chambers. In this respect, the rocks of the Gęsiniec Intrusion probably represent magmas that were not mixed, and each rock type represents the crystallization products of a distinct lower crustal magma chamber, providing information on possible differentiation processes that may happen in such chambers (Fig. 13). However, the lack of isotopic heterogeneity in the quartz diorite with the lowest $^{87}Sr/^{86}Sr_{295}$ (LPD), coupled with the presence of two contaminants in the higher $^{87}Sr/^{86}Sr_{295}$ quartz diorites (MD, LMGD, LCGD, MCGD-x), leaves us with an unsolved problem; namely, what is the reason for the relatively intermediate isotopic compositions in the whole suite of dioritic–tonalitic rocks? Is one of the contaminants that produced the within-suite isotopic variability the same as that responsible for the intermediate isotopic composition of diorites and tonalites in general? Alternatively, is the lack of isotopic heterogeneity due to a simple process of magma extraction by partial melting of basaltic lower crust? These questions might be impossible to answer unambiguously; however, comparison of rocks from the Gęsiniec Intrusion with those from other igneous rocks of the same age in the region may shed light on this problem.

The evolution of dioritic–tonalitic rocks in the Variscan orogenic setting

Ages similar to those of the Gęsiniec Intrusion (307–290 Ma) are found in both plutonic and volcanic complexes of Variscan age in Western, Central and Southern Europe (e.g. Finger *et al.*, 1997) suggesting that the Gęsiniec Intrusion represents part of a regional magmatic episode. Following major crustal thickening and subsequent post-collisional collapse during the Carboniferous–Permian (307–280 Ma), the Variscan orogenic belt in Europe underwent a major episode of extension, with associated formation of intramontane basins and widespread magmatic activity (Ziegler *et al.*, 2004), including intrusion of voluminous mafic magmas into the thinned lower crust. Crystallized remnants of these magmas are currently exposed as mafic layered intrusions predominantly in the Alpine area (Tribuzio *et al.*, 1999; Hermann *et al.*, 2001; Montanini & Tribuzio, 2001; Peressini *et al.*, 2007). The least evolved samples from these intrusions have isotopic signatures close to those of the depleted mantle. The most evolved but least voluminous rocks often have Nd and Sr isotopic compositions similar to those of the Gęsiniec Intrusion (Fig. 12), indicating that it is possible to produce evolved dioritic–tonalitic rocks by AFC process from originally mafic, mantle-derived magmas. However, at the same time, intrusion of those mafic magmas must have triggered extensive melting of the lower crust, as indicated by the presence of widespread granodioritic to

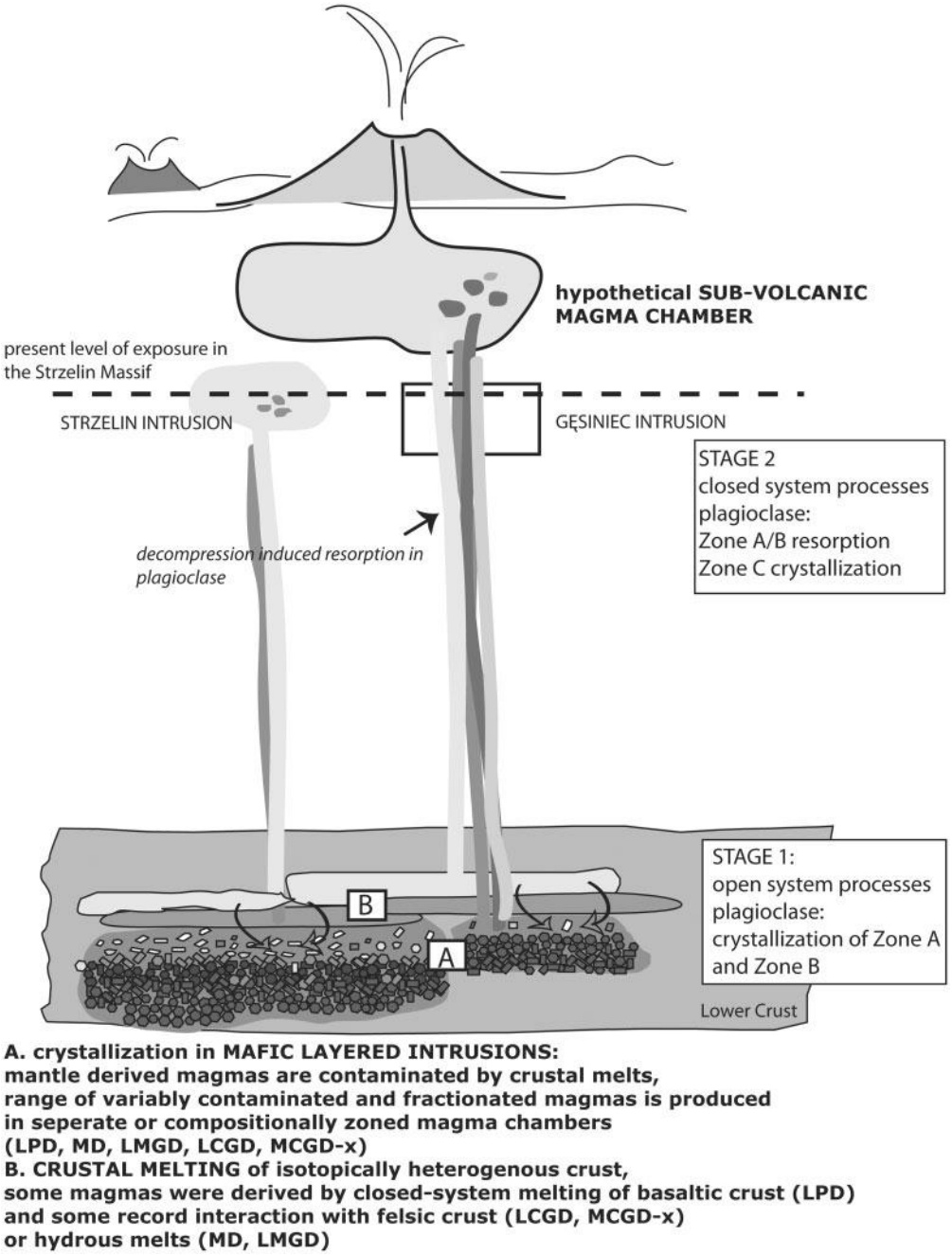

Fig. 13. Schematic illustration of a supposed source and processes that produced the range of dioritic–tonalitic rocks in the Gęsiniec Intrusion.

granitic intrusions and associated volcanic rocks of Carboniferous–Permian age. As modeled by Annen *et al.* (2006), it is possible to produce small amounts of quartz dioritic magmas by partial melting of lower crust with a basaltic composition. If we assume that the Gęsiniec quartz diorites with the lowest $^{87}Sr/^{86}Sr_{295}$ and the highest ε_{Nd295} (FGD, LPD) were derived from a mafic crustal source, such a crust would have a one-stage Nd model age of ~1·3 Ga and a two-stage Nd model age of ~1·8–2·1 Ga (for details see Table 8). Interestingly, the latter is in agreement with zircon Hf model ages from the Lachlan Fold Belt, which indicate a major episode of mafic crust formation in Gondwana at ~1·9 ± 0·1 Ga (Kemp *et al.*, 2006). If the dioritic–tonalitic magmas were in fact derived from ~1·9 ± 0·1 Ga mafic crust, this would suggest that such crust was an active and important component contributing to magmatism in different parts of Gondwana and should be taken into account in geochemical models of Variscan

Table 8: Depleted mantle Nd model ages (T_{DM}). 1 stage T_{DM} is calculated using $^{147}Sm/^{144}Nd$ ratio of the sample. 2 stage T_{DM} is calculated using $^{147}Sm/^{144}Nd$ of 0.15 and 0.16 (2nd and 3rd column respectively). 2 stage model assumes that the dioritic – tonalitic rocks were derived by melting of a basaltic crust with average $^{147}Sm/^{144}Nd$ ratios of basaltic rocks in ocean island (n = 147) and continental (n = 370) settings (GEOROC database)

	T_{DM} 1 stage	T_{DM} 2 stage	T_{DM} 2 stage
FGD	1285	1841	2125
LPD	1318	1830	2112
MD	1317	1894	2188
LMGD	1315	1842	2126
LCGD	1394	1968	2275

magmatic evolution. A larger isotope set of mineral data (e.g. O and Hf composition of zircons) is needed to confirm this hypothesis. Figure 13 shows possible settings in which the Gęsiniec magmas could be produced.

CONCLUSIONS

Whole-rock geochemistry is commonly used to reveal relationships between mafic and felsic rocks coexisting in single intrusions or intrusive complexes. Broadly linear or curved trends defined by rocks with variable major and trace element compositions are commonly interpreted in terms of fractional crystallization, accumulation of early crystallized phases, crustal assimilation or mixing with compositionally distinct magmas. Evidence of open-system processes is often preserved in crystal microstructures as resorption surfaces. However, only *in situ* trace element and isotopic analyses across such resorption surfaces can provide strong evidence that an open-system process took place.

In this study we have shown that a major resorption event identified in plagioclase (between Zone A + B and Zone C) and accompanied by a steady decrease in An content is not correlated with magma mixing or crustal contamination and is best explained by resorption as a result of decompression. In contrast, the consistent and significant variations in Sr isotopic composition within high-An cores (Zone A + B) together with rounded resorption of Zone A emphasize the importance of open-system processes that are not marked by drastic changes in An content or significant and complex resorption surfaces. Correlation of the core (Zone A + B)–rim (Zone C) resorption with decompression gives an opportunity to separately characterize the processes that occurred before and after emplacement. We suggest that the dioritic–tonalitic magmas evolved first in deep crustal magma chambers by contamination of water-rich melts with crustal components. Essentially, each quartz diorite type must have evolved separately and records different differentiation processes both in Zone A and B plagioclase and whole-rock composition.

It is now becoming increasingly clear that many granitic magmas represent the end result of complex processes of magma mixing, and represent mixtures of crystals formed in both juvenile and crust-derived magmas (Gagnevin *et al.*, 2005; Kemp *et al.*, 2007; Słaby *et al.*, 2007; Beard, 2008). Tonalitic–dioritic inclusions (enclaves) in granites are often considered to represent remnants of the juvenile (mantle-derived) component (e.g. Waight *et al.*, 2001). Our results from the Gęsiniec Intrusion suggest that the least evolved quartz diorites either represent homogenized hybrid material formed during differentiation of a mafic intrusion at depth or were derived by partial melting of old basaltic crust. This suggests that dioritic–tonalitic and granitic rocks may evolve separately in many orogenic provinces and might mingle with more felsic magmas only after their intrusion in the upper crust. In this scenario the enclaves still represent the mafic end-member in a mixing scheme, but instead of representing direct injections of primary melt from the mantle, they represent melts that have resided in a lower crustal magma chamber before upper crustal mixing. This may be a useful way of explaining why we do not find pristine basaltic enclaves with mantle-like compositions; the magmas have had time to evolve and be contaminated before mixing.

ACKNOWLEDGEMENTS

A.P. is grateful to Berit Wenzell (Institute for Geography and Geology, Copenhagen), Jürgen Koepke (Institute of Mineralogy, Hannover) and Magnus Johansson (Institute of Mineralogy, Hannover) for help during microprobe analyses. Jane Chadwick and Maria Jankowski are thanked for help with isotope laboratory chemistry. Helpful comments and discussions from Teresa Oberc-Dziedzic, Chris Hawkesworth, Francois Holtz and Jacek Puziewicz are acknowledged. The authors would like to gratefully acknowledge constructive reviews by Frank Tepley, Fritz Finger and anonymous reviewers, as well as very helpful comments of editor Wendy Bohrson, which significantly improved the quality of the manuscript. The work was supported by a Marie Curie fellowship to A.P. at the Danish Lithosphere Center funded by the Danskgrundforkningsfond and the Polish Committee for Scientific Research (KBN) grant 2 P04D01627 to A.P.

SUPPLEMENTARY DATA

Supplementary data for this paper are available at *Journal of Petrology* online.

REFERENCES

Aleksandrowski, P. & Mazur, S. (2002). Collage tectonics in the north-easternmost part of the Variscan Belt: the Sudetes, Bohemian Massif. In: Winchester, J. A., Pharoah, T. C. & Verniers, J. (eds). *Palaeozoic Amalgamation of Central Europe. Geological Society, London, Special Publications* **201**, 237–277.

Altherr, R., Henes-Klaiber, U., Hegner, E., Satir, M. & Langer, C. (1999). Plutonism in the Variscan Odenwald (Germany): from subduction to collision. *International Journal of Earth Sciences* **88**, 422–443.

Anders, E. & Grevesse, N. (1989). Abundances of the elements: meteoric and solar. *Geochimica et Cosmochimica Acta* **53**, 197–214.

Anderson, J. L. & Smith, D. R. (1995). The effects of temperature and f_{O2} on the Al-in-hornblende barometer. *American MIneralogist* **80**, 549–559.

Annen, C., Blundy, J. D. & Sparks, R. S. J. (2006). The genesis of intermediate and silicic magmas in deep crustal hot zones. *Journal of Petrology* **47**, 505–539.

Asrat, A., Barbey, P., Ludden, J. N., Reisberg, L., Gleizes, G. & Ayalew, D. (2004). Petrology and isotope geochemistry of the Pan-African Negash pluton, Northern Ethiopia: Mafic–felsic magma interactions during the construction of shallow-level calc-alkaline plutons. *Journal of Petrology* **45**, 1147–1179.

Bea, F., Montero, P. & Molina, J. F. (1999). Mafic precursors, peraluminous granitoids, and lamprophyres in the Avila batholith: a model for the generation of Variscan batholiths in Iberia. *Journal of Geology* **107**, 399–419.

Beard, J. S. (2008). Crystal–melt separation and the development of isotopic heterogeneities in hybrid magmas. *Journal of Petrology* **49**, 1027–1041.

Beard, J. S. & Lofgren, G. E. (1991). Partial melting of basaltic and andesitic greenstones and amphibolites under dehydration melting and watersaturated conditions at 1, 3, and 6·9 kilobars. *Journal of Petrology* **32**, 365–401.

Beddoe-Stephens, B. (1999). The Glen Tilt diorite: crystallization, petrogenesis and relation to granitic rocks. *Scottish Journal of Geology* **35**, 157–177.

Bindeman, I. N., Davi, A. M. & Drake, M. J. (1998). Ion microprobe study of plagioclase–basalt partition experiments at natural concentration levels of trace elements. *Geochimica et Cosmochimica Acta* **62**, 1175–1193.

Blundy, J. D. & Shimizu, N. (1991). Trace element evidence for plagioclase recycling in calc-alkaline magmas. *Earth and Planetary Science Letters* **102**, 178–191.

Castro, A., Corretgé, L. G., De La Rosa, J., Fernández, C., López, S., Gracía-Moreno, O. & Chacón, H. (2003). The appinite–migmatite complex of Sanabria, NW Iberian Massif, Spain. *Journal of Petrology* **44**, 1309–1344.

Christofides, G., Perugini, D., Koroneos, A., Soldatos, T., Poli, G., Eleftheriadis, G., Del Moro, A. & Neiva, A. M. (2007). Interplay between geochemistry and magma dynamics during magma interaction: An example from the Sithonia Plutonic Complex (NE Greece). *Lithos* **95**, 243–266.

Cortesogno, L., Cassinis, G., Dallagiovanna, G., Gaggero, L., Oggiano, G., Ronchi, A., Seno, S. & Vanossi, M. (1998). The Variscan post-collisional volcanism in Late Carboniferous–Permian sequences of Ligurian Alps, Southern Alps and Sardinia: a synthesis. *Lithos* **45**, 305–328.

Davidson, J. P., Morgan, D. J., Charlier, B. L. A., Harlou, R. & Hora, J. M. (2007). Microsampling and isotopic analysis of igneous rocks: Implications for the study of magmatic systems. *Annual Review of Earth and Planetary Sciences* **35**, 273–311.

Elburg, M. A. (1996). Evidence of equilibration between microgranitoid enclaves and host granodiorite, Warburton Granodiorite, Lachlan Fold Belt, Australia. *Lithos* **38**, 1–22.

Finger, F., Roberts, M. P., Haunschmid, B., Schermaier, A. & Steyrer, H. P. (1997). Variscan granitoids of Central Europe: their typology, potential sources and tectonothermal relations. *Mineralogy and Petrology* **61**, 67–96.

Gagnevin, D., Daly, J. S., Poli, G. & Morgan, D. (2005). Microchemical and Sr isotopic investigation of zoned K-feldspar megacrysts: Insights into the petrogenesis of a granitic system and disequilibrium crystal growth. *Journal of Petrology* **46**, 1689–1724.

Gagnevin, D., Waight, T. E., Daly, J. S., Poli, G. & Conticelli, S. (2007). Insights into magmatic evolution and recharge history in Capraia Volcano (Italy) from chemical and isotopic zoning in plagioclase phenocrysts. *Journal of Volcanology and Geothermal Research* **168**, 28–54.

Ginibre, C., Worner, G. & Kronz, A. (2007). Crystal zoning as an archive for magma evolution. *Elements* **3**, 261–266.

Hermann, J., Müntener, O. & Günther, D (2001). Differentiation of mafic magma in a continental crust-to-mantle transition zone. *Journal of Petrology* **42**, 189–206.

Hibbard, M. J. (1981). The magma mixing origin of mantled feldspars. *Contributions to Mineralogy and Petrology* **76**, 158–170.

Janoušek, V., Bowes, D. R., Rogers, G., Farrow, C. M. & Jelinek, E. (2000). Modelling diverse processes in the petrogenesis of a composite batholith: the Central Bohemian Pluton, Central European Hercynides. *Journal of Petrology* **41**, 511–543.

Janoušek, V., Braithwaite, C. J. R., Bowes, D. R. & Gerdes, A. (2004). Magma-mixing in the genesis of Hercynian calc-alkaline granitoids: an integrated petrographic and geochemical study of the Sázava intrusion, Central Bohemian Pluton, Czech Republic. *Lithos* **78**, 67–99.

Johannes, W. & Holtz, F. (1996). The tonalite system Qz–Ab–An. In: Johannes, W. & Holtz, F. (eds) *Petrogenesis and Experimental Petrology of Granitic Rocks*. Berlin: Springer, pp. 202–228.

Johannes, W., Koepke, J. & Behrens, H. (1994). Partial melting reactions of plagioclase and plagioclase bearing systems. In: Parson, I. (ed.) *Feldspars and their Reactions*. Dordrecht: Kluwer, pp. 161–194.

Jung, S., Hoernes, S. & Mezger, K. (2002). Synorogenic melting of mafic lower crust: constraints from geochronology, petrology and Sr, Nd, Pb and O isotope geochemistry of quartz diorites (Damara orogen, Namibia). *Contributions to Mineralogy and Petrology* **143**, 551–566.

Kemp, A. I. S., Hawkesworth, C. J., Paterson, B. A. & Kinny, P. D. (2006). Episodic growth of the Gondwana supercontinent from hafnium and oxygen isotopes in zircon. *Nature* **439**, 580–583.

Kemp, A. I. S., Hawkesworth, C. J., Foster, G. L., Paterson, B. A., Woodhead, J. D., Hergt, J. M., Gray, C. M. & Whitehouse, M. J. (2007). Magmatic and crustal differentiation history of granitic rocks from Hf–O isotopes in zircon. *Science* **315**, 980–983.

Košler, J. (2001). Laser-ablation ICPMS study of metamorphic minerals and processes. *Laser-Ablation-ICPMS in the Earth Sciences*, 185–202.

Kystol, J. & Larsen, L. M. (1999). Analytical procedure in the rock geochemical laboratory of the Geological Survey of Denmark and Greenland. *Geology of Greenland Survey Bulletin* **184**, 59–62.

Lange, U., Bröcker, M., Armstrong, R.,Żelaźniewicz, A., Trapp, E. & Mezgner, K. (2005). The orthogneisses of the Orlica–Śnieżnik complex (West Sudetes, Poland): geochemical characteristics, the importance of pre-Variscan migmatization and constraints on the cooling history. *Journal of the Geological Society, London* **162**, 973–984.

Leake, B. E., Woolley, A. R., Arps, C. E. S. *et al.* (1997). Nomenclature of amphiboles: report of the Subcommittee on amphiboles of the

International Mineralogical Association Commission on New Minerals and Mineral Names. *Mineralogical Magazine* **61**, 295–321.

Lesher, C. E. (1994). Kinetics of Sr and Nd exchange in silicate liquids—theory, experiments, and applications to uphill diffusion, isotopic equilibration, and irreversible mixing of magmas. *Journal of Geophysical Research—Solid Earth* **99**, 9585–9604.

Luais, B., Telouk, P. & Albarède, F. (1997). Precise and accurate neodymium isotopic measurements by plasma-source mass spectrometry. *Geochimica et Cosmochimica Acta* **61**, 4847–4854.

Ludwig, K. R. (2004). Isoplot/Ex: A Geochronological Toolkit for Microsoft Excel. *Berkeley Geochronology Center, Special Publication* 1a (rev. 3).

Mazur, S., Aleksandrowski, P., Kryza, R. & Oberc-Dziedzic, T. (2006). The Variscan Orogen in Poland. *Geological Quarterly* **50**, 89–118.

Montanini, A. & Tribuzio, R. (2001). Gabbro-derived granulites from the Northern Apennines (Italy): Evidence for lower-crustal emplacement of tholeiitic liquids in post-Variscan times. *Journal of Petrology* **42**, 2259–2277.

Nakamura, M. & Shimakita, S. (1998). Dissolution origin and syn-entrapment compositional change of melt inclusion in plagioclase. *Earth and Planetary Science Letters* **161**, 119–133.

Nelson, S. T. & Montana, A. (1992). Sieved-textured plagioclase in volcanic rocks produced by rapid decompression. *American Mineralogist* **77**, 1242–1249.

Oberc-Dziedzic, T. (1999*a*). The metamorphic and structural development of gneisses and older schist series in the Strzelin crystalline massif (Fore-Sudetic Block, SW Poland). *Mineralogical Society of Poland—Special Papers* **14**, 10–21.

Oberc–Dziedzic, T. (1999*b*). The geology of Strzelin Granitoids (Fore-Sudetic Block, SW Poland). *Mineralogical Society of Poland—Special Papers* **14**, 22–32.

Oberc-Dziedzic, T. (2002). Polycycle structure of the tonalite–diorite dykes in the Strzelin massif: a result of magmatic differentiation or separated magmatic pulses? *Mineralogical Society of Poland—Special Papers* **20**, 159–161.

Oberc-Dziedzic, T., Klimas, K., Kryza, R. & Fanning, C. M. (2003). SHRIMP U-Pb zircon geochronology of the Strzelin gneiss, SW Poland: evidence for a Neoproterozoic thermal event in the Fore-Sudetic Block, Central European Variscides. *International Journal of Earth Sciences* **92**, 701–711.

Oberc-Dziedzic, T. & Madej, S. (2002). The Variscan overthrust of the Lower Palaeozoic gneiss unit on the Cadomian basement in the Strzelin and Lipowe Hills massifs, Fore-Sudetic Blocck, SW Poland; is this part of the East–West Sudetes boundary? *Geologia Sudetica* **34**, 39–58.

Oberc–Dziedzic, T., Pin, C., Duthou, J. L. & Couturie, J. P. (1996). Age and origin of Strzelin granitoids (Fore-Sudetic Block, SW Poland): $^{87}Rb/^{86}St$ data. *Neues Jahrbuch für Mineralogie, Abhandlungen* **171**, 187–198.

Pearce, N. J. G., Perkins, W. T., Westgate, J. A., Gorton, M. P., Jackson, S. E., Neal, C. R. & Chenery, S. P. (1997). A compilation of new and published major and trace element data for NIST SRM 610 and NIST SRM 612 Glass Reference Materials. *Geostandards Newsletter* **21**, 115–144.

Peressini, G., Quick, J. E., Sinigoi, S., Hofmann, A. W. & Fanning, M. (2007). Duration of a large mafic intrusion and heat transfer in the lower crust: a SHRIMP U–Pb zircon study in the Ivrea–Verbano Zone (Western Alps, Italy). *Journal of Petrology* **48**, 1185–1218.

Petford, N., Cruden, A. R., McCaffrey, K. J. W. & Vigneresse, J.-L. (2000). Granite magma formation, transport and emplacement in the Earth's crust. *Nature* **408**, 669–673.

Pietranik, A., Koepke, J. & Puziewicz, J. (2006). Crystallization and resorption in plutonic plagioclase: Implications on the evolution of granodiorite magma (Gesiniec granodiorite, Strzelin Crystalline Massif, SW Poland). *Lithos* **86**, 260–280.

Pinarelli, L., Moro, A., Boriani, A. & Caironi, V. (2002). Sr, Nd isotope evidence for an enriched mantle component in the origins of the Hercynian gabbro–granite series of the 'Serie dei Laghi' (Southern Alps, NW Italy). *European Journal of Mineralogy* **14**, 403–415.

Rapp, R. P. & Watson, E. B. (1995). Dehydration melting of metabasalt at 8–32 kbar—implications for continental growth and crust–mantle recycling. *Journal of Petrology* **36**, 891–931.

Roberts, M. P., Pin, C., Clemens, J. D. & Paquette, J.-L. (2000). Petrogenesis of mafic to felsic plutonic rocks associations: the calc-alkaline Quérigut Complex, French Pyrenees. *Journal of Petrology* **41**, 809–844.

Romer, R. L., Forster, H. J. & Breitkreuz, C. (2001). Intracontinental extensional magmatism with a subduction fingerprint: the late Carboniferous Halle Volcanic Complex (Germany). *Contributions to Mineralogy and Petrology* **141**, 201–221.

Słaby, E., Galbarczyk-Gąsiorowska, L., Seltmann, R. & Müller, A. (2007). Alkali feldspar megacryst growth: Geochemical modelling. *Mineralogy and Petrology* **89**, 1–29.

Smith, J. V. & Brown, W. L. (1988). *Feldspar Minerals*. Heidelberg: Springer, 828 pp.

Sun, S. S. & McDonough, W. F. (1989). Chemical and isotopic systematics of oceanic basalts; implications for mantle composition and processes. In: Saunders, A. D. & Norry, M. J. (eds). *Magmatism in the Ocean Basins. Geological Society, London, Special Publications* **42**, 313–345.

Tepley, F. J. & Davidson, J. P. (2003). Mineral-scale Sr-isotope constraints on magma evolution and chamber dynamics in the Rum layered intrusion, Scotland. *Contributions to Mineralogy and Petrology* **145**, 628–641.

Tribuzio, R., Thirlwall, M. F. & Messiga, B. (1999). Petrology, mineral and isotope geochemistry of the Sondalo gabbroic complex (Central Alps, Northern Italy): implications for the origin of post-Variscan magmatism. *Contributions to Mineralogy and Petrology* **136**, 48–62.

Tsuchiyama, A. (1985). Dissolution kinetics of plagioclase in melt of the system diopside–albite–anorthite, and the origin of dusty plagioclase in andesites. *Contributions to Mineralogy and Petrology* **89**, 1–16.

Turniak, K., Tichomirowa, M. & Bombach, K. (2006). Pb-evaporation zircon ages of post-tectonic granitoids from the Strzelin Massif (SW Poland). *Mineralogia Polonica—Special Papers* **29**, 212–215.

Vance, J. A. (1965). Zoning in igneous plagioclase: patchy zoning. *Journal of Geology* **73**, 636–651.

Waight, T. E., Maas, R. & Nicholls, I. A. (2000). Fingerprinting feldspar phenocrysts using crystal isotopic composition stratygraphy: implications for crystal transfer and magma mingling in S-type granites. *Contributions to Mineralogy and Petrology* **139**, 227–239.

Waight, T. E., Maas, R. & Nicholls, I. A. (2001). Geochemical investigations of microgranitoid enclaves in the S-type Cowra Granodiorite, Lachlan Fold Belt, SE Australia. *Lithos* **56**, 165–186.

Waight, T. E., Baker, J. A. & Willigers, B. J. A. (2002). Rb isotope dilution analyses by MC-ICPMS using Zr to correct for mass fractionation: towards improved Rb–Sr geochronology? *Chemical Geology* **186**, 99–116.

Zhao, Z. F., Zheng, Y. F., Wei, C. S. & Wu, Y. B. (2007). Post-collisional granitoids from the Dabie orogen in China: Zircon U–Pb age, element and O isotope evidence for recycling of subducted continental crust. *Lithos* **93**, 248–272.

Ziegler, P. A., Schumacher, M. E., Dèzes Van Wees, J.-D. & Cloetingh, S. (2004). Post-Variscan evolution of the lithosphere in the Rhine Graben area: constraints from subsidence modelling. In: Wilson, M., Neumann, E.-R., Davies, G. R., Timmerman, M. J., Heeremans, M. & Larsen, B. T. (eds). *Permo-Carboniferous Magmatism and Rifting in Europe. Geological Society, London, Special Publications* **223**, 289–317.

Table A1: Precision and accuracy of trace element concentrations determined by LA-ICPMS, based on replicate analyses of standard SRM NIST 612 glass as unknown and limits of detection

Analysed isotope of the element	Accuracy (mean of 16 measurements)	Reproducibility (± 2SD)	Limit of detection	SRM 612 (Pearce *et al.*, 1997)
^{24}Mg	70·6	9·9	19·0	77·44
^{47}Ti	48·1	8·7	14·6	42·03
^{55}Mn	38·4	5·0	3·0	45·81
^{88}Sr	76·2	6·9	2·1	76·01
^{138}Ba	37·7	3·0	2·5	39·25
^{139}La	35·8	1·3	1·1	36·21
^{140}Ce	38·4	4·6	0·1	43·54
^{153}Eu	34·4	2·8	0·6	35·69
^{208}Pb	39·0	7·8	0·2	50·75

All values are in ppm.